Research Square

Preprints are preliminary reports that have not undergone peer review.
They should not be considered conclusive, used to inform clinical practice,
or referenced by the media as validated information.

Thermal buckling and mode jumping analysis in compressed composite profiles

Katarzyna Falkowicz

k.falkowicz@pollub.pl

Lublin University of Technology

Pawel Wysmulski

Lublin University of Technology

Article

Keywords: thermal buckling, thermal analysis, axial compression, mode jumping, composite

Posted Date: September 22nd, 2026

DOI: https://doi.org/10.21203/rs.3.rs-10957211/v1

License: This work is licensed under a Creative Commons Attribution 4.0 International License.
Read Full License

Additional Declarations: No competing interests reported.

Version of Record: A version of this preprint was published at Scientific Reports on November 4th, 2026.
See the published version at https://doi.org/10.1038/s41598-026-77885-9.

Thermal buckling and mode jumping analysis in compressed composite profiles

Katarzyna Falkowicz*, Pawel Wysmulski

Department of Machine Design and Mechatronics, Faculty of Mechanical Engineering, Lublin University of Technology, Nadbystrzycka 36, 20-618 Lublin, Poland, *email: k.falkowicz@pollub.pl

Keywords: *thermal buckling, thermal analysis, axial compression, mode jumping, composite profiles*

Abstract

This paper examines the thermomechanical behavior of composite materials under axial compression across a wide temperature range, focusing on buckling mode transitions. Experimental tests were conducted using a servo-hydraulic MTS system at temperatures from -20°C to 80°C. Load-displacement and load-deflection data were collected via a 3D DIC system, ensuring accurate characterization of the buckling response. The results reveal a significant impact of temperature on the critical load and buckling mode evolution. Mode transitions at higher temperatures as well as during the loading were marked by changes in the number of half-waves in the buckling pattern. Lower temperatures increased stiffness and critical loads, while higher temperatures induced ductile behavior, reducing the critical load and allowing larger displacements before failure. These findings highlight the crucial role of thermal effects in composite stability and reliability, aiding the design of aerospace and high-performance structures.

1. Introduction

Thin-walled composite structures play a crucial role in modern aerospace [1–5], automotive, railway [6] and construction industries [7,8] due to their exceptional mechanical properties, such as a high strength-to-weight ratio and corrosion resistance. However, a key challenge in their operation is ensuring structural reliability under varying temperature conditions, which can significantly affect deformation mechanisms and the critical buckling load. Numerous significant research studies have been conducted on buckling [9–12] and post-buckling behavior of composite plates [13–16] or profiles with different cross-sectional shapes, but these studies have predominantly been performed at room temperature [17–19]. In contrast, investigations considering temperature effects remain limited. The phenomenon of thermal buckling, although well-documented for conventional materials [20,21], requires further research in the context of composites with complex layered structures. The novelty of the proposed approach lies in the detailed analysis of buckling mode transitions across a wide temperature range, enabling a better understanding of the transition process between different deformation modes and their impact on structural durability.

Among composite materials, fiber-reinforced polymers (FRP) stand out, particularly carbon-epoxy composites (CFRP) and glass-epoxy composites (GFRP). GFRP, being a more cost-effective option, is widely used in less demanding environments. However, its mechanical

properties deteriorate significantly at high temperatures, limiting its application in critical structures [22].

Previous studies on the effect of temperature on the buckling of composites have primarily focused on GFRP materials. Research published in [23] demonstrated that the transverse elastic modulus of GFRP laminates decreased by 48% at 200°C, while tensile strength dropped by 40%. Other studies indicate a significant reduction in tensile strength with increasing temperature [24]. Chowdhury et al. confirmed that the tensile strength of unidirectional GFRP laminates declines sharply above the glass transition temperature, limiting their application in high-temperature environments [25]. The study [26] revealed that high temperatures lead to the earlier onset of local buckling, significantly reducing structural load-bearing capacity and increasing the risk of failure. The phenomenon of mode jumping, where a structure shifts its buckling modes due to thermal loading, has also been observed in CFRP structures. However, further research is needed, particularly to explore its potential application in adaptive aerospace structures.

Preliminary studies conducted in paper [27] showed that at low temperatures, such as -20°C, composite omega-section profiles exhibit increased stiffness and higher buckling resistance, resulting in more complex deformation patterns with multiple half-waves. At higher temperatures, above 60°C, the material's elastic modulus significantly decreases, leading to simpler but less stable buckling modes and an earlier attainment of the critical buckling load [20]. Deformation asymmetry at high temperatures increases the risk of local damage, directly affecting the reliability and operational safety of composite structures.

Mode jumping

Mode jumping in heated composite materials is a key phenomenon that arises under combined thermomechanical loads, particularly during buckling. It manifests as a sudden change in the mode shape of the composite structure, which can enhance adaptability in specific applications, such as aerospace engineering. However, from an operational and reliability standpoint, this behavior introduces both opportunities and risks.

In the context of operational performance, mode jumping can offer significant advantages by enabling local morphing and structural adaptability, which are crucial for improving the efficiency and functionality of aerospace structures [26]. This adaptability allows structures to respond dynamically to changing thermal conditions, potentially reducing material fatigue and extending service life. Research by [26] revealed that thermal loads can induce a transition to a new buckling mode, often characterized by an increase in the number of half-waves in the structure. Their subsequent study [28] further confirmed that mode jumping is driven by complex interactions between thermal and mechanical forces, resulting in behaviors that are highly dependent on the specific loading conditions.

From a reliability perspective, while mode jumping enhances structural flexibility, it can also complicate the prediction and monitoring of stability under variable thermal conditions. Chen et al. [29] highlighted that thermal stresses significantly impact modal characteristics, posing a greater influence than the material property variations caused by heating. These unpredictable shifts in buckling modes can affect the long-term durability of composite materials and increase the risk of failure if not carefully monitored and controlled.

Thus, understanding the balance between adaptability and reliability is crucial for the safe and efficient exploitation of composite materials. Continued research into mode jumping is essential to mitigate its risks and harness its potential, ensuring both operational performance and structural integrity are maintained over extended service periods.

The novelty of this study lies in the analysis of the effect of temperature on the real-time transition of buckling modes and the identification of transition mechanisms as a function of temperature. The findings of this research have significant practical implications, enabling better design and optimization of structural components, particularly those operating under variable environmental conditions where reliability and safety play a crucial role.

The objective of this article is not only to enhance the understanding of the influence of temperature on buckling but also to formulate recommendations for the operation of composite structures to minimize failure risks and improve their durability and reliability.

The physical phenomenon addressed in this study is the temperature-dependent evolution of buckling modes in thin-walled CFRP profiles, manifested as real-time mode jumping under axial compression. Although the thermal degradation of stiffness in composites is well documented, the dynamic instability pathway—specifically how temperature alters the sequence of deformation shapes, the redistribution of half-waves, and the abrupt transitions between competing buckling modes—has not been sufficiently examined in the literature, particularly for open-section profiles. The present work fills this gap by capturing the deformation process through high-resolution DIC and correlating the observed mode transitions with temperature-induced changes in anisotropic stiffness components. This provides a deeper physical understanding of the instability mechanisms governing composite structures subjected to thermomechanical loads.

In summary, understanding the effect of temperature on the buckling behavior of CFRP composites and their potential mechanical degradation is essential for ensuring the reliability and operational safety of these materials in changing environmental conditions. Addressing this research gap will facilitate the design of structures with high thermal resistance and enhanced durability.

2. The research subject and methodology

2.1. Specimen

The study examined an Z-profile with an open cross-section, constructed from a carbon-epoxy composite material – CFRP (the Gurit EP 137 prepreg), a composite material with anisotropic properties, using the autoclave manufacturing method. Fabrication was carried out by WIT-Composites (Poland), a company specializing in high-precision composite manufacturing. All specimens were produced under controlled conditions to ensure dimensional accuracy and consistency across the test series. The complete curing cycle parameters have been explained in publications [30,31]. These types of structures are the most basic elements of load-bearing structures used in aerospace and other technical sectors. The mechanical properties of this material were determined according to the standard tests and presented in Table 2.1 as well as in [32,33]. For the test temperature of –20 °C, due to technical difficulties during the experiment and an insufficient number of valid specimens, only two mechanical properties - the in-plane shear modulus (G_{12}) and in-plane shear strength (X_{shr})

could be successfully determined. The remaining properties (such as E_1, E_2, ν_{12}, and tensile/compressive strength) could not be evaluated under these conditions.

TABLE 2.1. Mechanical and strength properties of CFRP material

Temp.	Young's modulus	Young's modulus	Poisson's ratio	Kirchhoff modulus	Tensile Strength X_{T1}	Tensile Strength X_{T2}	Shear Strength X_{shr}	Compressive Strength X_{C1}	Compressive Strength X_{C2}
T	E_1	E_2	ν_{12}	G_{12}	FTU (0°)	FTU (90°)	FSU (45°)	FCU (0°)	FCU (90°)
°C	MPa	MPa	MPa	MPa	MPa	MPa	MPa	MPa	MPa
-20	-	-	-	5654.6	-	-	161.9	-	-
20	118317.1	8339.4	0.31	4596	1781.4	49.1	137.5	707.6	115.5
40	120981.4	7974.9	0.32	4346.1	1511.3	50.7	118.2	706.8	113.2
60	124339.4	7323.2	0.34	3453.9	1387.3	49	96.1	484.8	77.8
80	127962.3	5457.4	0.39	1908.1	1281.2	38.5	80.7	358.3	65.2

The dimensions of the tested samples and the chosen stacking sequence [0/0/45/-45/90/90/-45/45/0/0] are presented in Figure 2.1. This symmetric and balanced configuration incorporates multiple fiber orientations, including 0°, ±45°, and 90°, which are commonly used in aerospace-grade laminates. The outer 0° plies enhance axial stiffness and load-bearing capacity in the primary loading direction, while the ±45° layers improve shear resistance and energy dissipation under compressive loads. The central 90° plies contribute to transverse stiffness and influence the coupling behavior between in-plane and out-of-plane responses. The chosen layout allows for the activation and evaluation of potential thermomechanical couplings (e.g., *Bending-Twisting*) under varying thermal conditions. Additionally, it enables the analysis of temperature-induced degradation mechanisms, such as matrix softening, fiber–matrix debonding, and local instabilities. Overall, this laminate design is well-suited for analyzing both global and local buckling phenomena as well as postbuckling behavior in thermally loaded composite structures and what is more except for a few rare cases, composite laminates used in aircraft structures are presently certified only if they are balanced and symmetric [34], which allows them to exhibit either uncoupled stiffness properties [35,36] or *Bending-Twisting* coupling [37].

According to the classical lamination theory (CLT), which is more often expressed using compact notation describes well-known ABD relation [38]:

$$\begin{Bmatrix} N \\ M \end{Bmatrix} = \begin{bmatrix} A & B \\ B & D \end{bmatrix} \begin{Bmatrix} \varepsilon \\ \kappa \end{Bmatrix} \tag{2.1}$$

where: N and M – internal forces and moments; ε and the mid-plane κ – strains and curvatures of the laminate respectively; A,B,D – are the stiffness matrices: extensional [A], coupling [B] and bending [D]. As well as referred to defined previously subscript notation by the Engineering Sciences Data Unit (ESDU, 1994) and extended later by Ch. York [39], this configuration can be written as $A_sB_0D_F$ and can be described as an B-T (*Bending-Twisting*) laminate [40]. It is mean that *Bending* causes a *Twisting* effect. The elements of the extensional stiffness matrix [A] are simple or specially orthotropic, i.e.:

$$\begin{bmatrix} A_{11} & A_{12} & 0 \\ sym. & A_{22} & 0 \\ sym. & sym. & A_{66} \end{bmatrix} \tag{2.2}$$

the coupling matrix [B] is null and the bending stiffness matrix [D] are finite, i.e.:

$$\begin{bmatrix} D_{11} & D_{12} & D_{16} \\ sym. & D_{22} & D_{26} \\ sym. & sym. & D_{66} \end{bmatrix} \tag{2.3}$$

The elements of stiffness matrices can be calculated from the well know relationships:

$$\begin{aligned} A_{ij} &= \sum_{k=1}^{n} Q'_{ij}\,(z_k - z_{k-1}) \\ B_{ij} &= \frac{\sum_{k=1}^{n} Q'_{ij}\,(z_k^2 - z_{k-1}^2)}{2} \\ D_{ij} &= \frac{\sum_{k=1}^{n} Q'_{ij}\,(z_k^3 - z_{k-1}^3)}{3} \end{aligned} \tag{2.4}$$

where the transformed reduced stiffness terms in Eq. (2.4) are given by:

$$\begin{gathered} Q'_{11} = Q_{11}cos^4\theta + 2(Q_{12} + 2Q_{66})cos^2\theta sin^2\theta + Q_{22}sin^4\theta \\ Q'_{12} = Q'_{21} = (Q_{11} + Q_{22} - 4Q_{66})cos^2\theta sin^2\theta + Q_{12}(cos^4\theta + sin^4\theta) \\ Q'_{16} = Q'_{61} = \{(Q_{11} - Q_{22} - 2Q_{66})cos^2\theta + (Q_{12} - Q_{22} + 2Q_{66})sin^2\theta\}cos\theta sin\theta \\ Q'_{22} = Q_{11}sin^4\theta + 2(Q_{12} + 2Q_{66})cos^2\theta sin^2\theta + Q_{22}cos^4\theta \\ Q'_{26} = Q'_{62} = \{(Q_{11} - Q_{12} - 2Q_{66})sin^2\theta + (Q_{12} - Q_{22} + 2Q_{66})cos^2\theta\}cos\theta sin\theta \\ Q'_{66} = (Q_{11} + Q_{22} - 2Q_{12} - 2Q_{66})cos^2\theta sin^2\theta + Q_{66}(cos^4\theta + sin^4\theta) \end{gathered} \tag{2.5}$$

where θ is play orientations and the reduced stiffness terms are given by:

$$\begin{gathered} Q_{11} = \frac{E_1}{(1 - \nu_{12}\nu_{21})} \\ Q_{12} = \frac{\nu_{12}E_2}{(1 - \nu_{12}\nu_{21})} = \frac{\nu_{21}E_1}{(1 - \nu_{12}\nu_{21})} \\ Q_{22} = \frac{E_2}{(1 - \nu_{12}\nu_{21})} \\ Q_{66} = G_{12} \end{gathered} \tag{2.6}$$

The ABD matrices for this designs, using the above formulas and material properties from Table 21.1 may be readily calculated as:

For 20°

$$\begin{Bmatrix} N_x \\ N_y \\ N_{xy} \\ M_x \\ M_y \\ M_{xy} \end{Bmatrix} = \begin{bmatrix} 64.443 & 12.995 & 0 & 0 & 0 & 0 \\ 12.995 & 42.297 & 0 & 0 & 0 & 0 \\ 0 & 0 & 14.992 & 0 & 0 & 0 \\ 0 & 0 & 0 & 8.443 & 0.667 & 0.221 \\ 0 & 0 & 0 & 0.667 & 1.283 & 0.221 \\ 0 & 0 & 0 & 0.221 & 0.221 & 0.834 \end{bmatrix} \begin{Bmatrix} \varepsilon_x \\ \varepsilon_y \\ \gamma_{xy} \\ \kappa_x \\ \kappa_y \\ \kappa_{xy} \end{Bmatrix}$$

For 40°

$$\begin{Bmatrix} N_x \\ N_y \\ N_{xy} \\ M_x \\ M_y \\ M_{xy} \end{Bmatrix} = \begin{bmatrix} 65.562 & 13.297 & 0 & 0 & 0 & 0 \\ 13.297 & 42.806 & 0 & 0 & 0 & 0 \\ 0 & 0 & 15.079 & 0 & 0 & 0 \\ 0 & 0 & 0 & 8.623 & 0.679 & 0.228 \\ 0 & 0 & 0 & 0.679 & 1.266 & 0.228 \\ 0 & 0 & 0 & 0.228 & 0.228 & 0.827 \end{bmatrix} \begin{Bmatrix} \varepsilon_x \\ \varepsilon_y \\ \gamma_{xy} \\ \kappa_x \\ \kappa_y \\ \kappa_{xy} \end{Bmatrix}$$

For 60°

$$\begin{Bmatrix} N_x \\ N_y \\ N_{xy} \\ M_x \\ M_y \\ M_{xy} \end{Bmatrix} = \begin{bmatrix} 66.688 & 13.881 & 0 & 0 & 0 & 0 \\ 13.881 & 43.124 & 0 & 0 & 0 & 0 \\ 0 & 0 & 14.825 & 0 & 0 & 0 \\ 0 & 0 & 0 & 8.840 & 0.702 & 0.236 \\ 0 & 0 & 0 & 0.702 & 1.221 & 0.236 \\ 0 & 0 & 0 & 0.236 & 0.236 & 0.780 \end{bmatrix} \begin{Bmatrix} \varepsilon_x \\ \varepsilon_y \\ \gamma_{xy} \\ \kappa_x \\ \kappa_y \\ \kappa_{xy} \end{Bmatrix}$$

For 80°

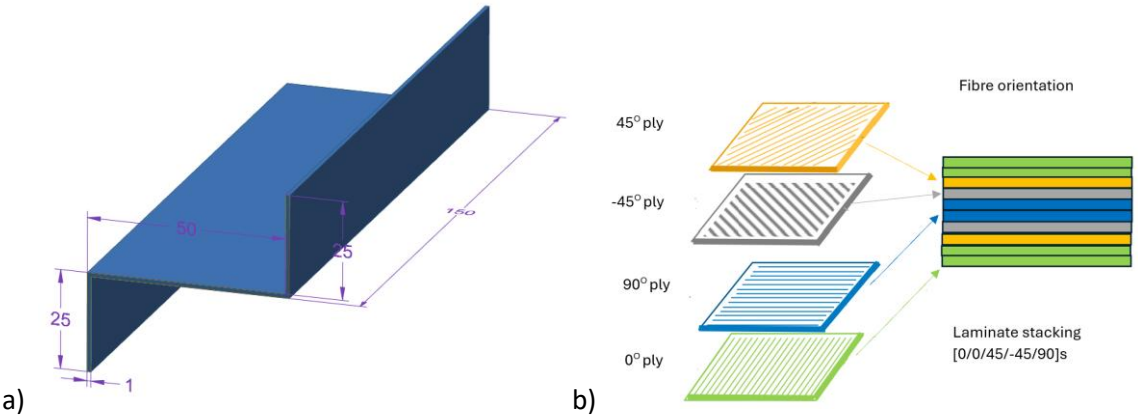
$$\begin{Bmatrix} N_x \\ N_y \\ N_{xy} \\ M_x \\ M_y \\ M_{xy} \end{Bmatrix} = \begin{bmatrix} 67.239 & 14.380 & 0 & 0 & 0 & 0 \\ 14.380 & 42.579 & 0 & 0 & 0 & 0 \\ 0 & 0 & 14.146 & 0 & 0 & 0 \\ 0 & 0 & 0 & 9.052 & 0.709 & 0.247 \\ 0 & 0 & 0 & 0.709 & 1.079 & 0.247 \\ 0 & 0 & 0 & 0.247 & 0.247 & 0.689 \end{bmatrix} \begin{Bmatrix} \varepsilon_x \\ \varepsilon_y \\ \gamma_{xy} \\ \kappa_x \\ \kappa_y \\ \kappa_{xy} \end{Bmatrix}$$

(2.7)

where: $A_{16}= A_{26}=0$; $B_{ij}=0$; $D_{ij}\neq 0$

All calculations were performed using an algorithm based on the equations described above.

It is worth noting that non-symmetric laminates, which are commonly associated with mechanically coupled behaviour, are still largely avoided in engineering practice in favor of symmetric laminate, primarily due to the perceived challenges in analysis and structural response. Nevertheless, the rule of symmetry merely ensures that the coupling matrix [B] in Eq. (2.1) equals zero, which can lead to compromised buckling performance [41]. In fact, most fully uncoupled laminates are non-symmetric by nature.



a) b)

FIGURE 2.1. a) Geometry and dimension of tested profiles, b) the example of cross-section of chosen configuration

2.2. Experimental tests

Axial compression tests were conducted using a servo-hydraulic MTS (Materials Test Systems) machine across a broad temperature range, spanning from -20°C to 80°C, with intervals of approximately 20°C. The tests were performed at a constant displacement rate of 1 mm/min. The setup for temperature control is depicted in Figures 2.2, showing a heating system capable of reaching 80°C and a cooling system based on liquid nitrogen for achieving the lowest

temperature of -20°C. The experiment was first conducted at the reference temperature of +20 °C, after which tests were repeated at −20 °C, +40 °C, +60 °C, and +80 °C using a climatic chamber equipped with integrated heating and nitrogen-based cooling. Once the chamber reached the target temperature, each specimen was conditioned for approximately 15 minutes to allow the laminate to reach a uniform thermal state.

Temperature control was monitored using the chamber's built-in calibrated sensors, which guaranteed thermal stability during testing. Moreover, thermocouples were attached directly to the external surface of each specimen, enabling continuous monitoring of the actual specimen temperature rather than relying solely on chamber readings. This ensured that no significant temperature gradients were present during testing.

During the tests, load-displacement data were collected directly from the testing machine, while load-deflection measurements were obtained through the GOM ARAMIS system, which utilizes the 3D Digital Image Correlation (DIC) technique [42]. At each temperature level, the buckling behavior was observed and documented. The boundary conditions applied to the test samples are illustrated in Figure 2.3.b. The specimens were simply supported at both ends using round supports mounted in the grips of the testing machine. The Authors are fully aware of the sensitivity of buckling behaviour to eccentricity and end-fixity conditions, which has been demonstrated in their prior studies [43–45]. To minimize setup errors, machine calibration was performed before each test, and specimens were inspected for cutting imperfections and initial out-of-straightness prior to mounting.

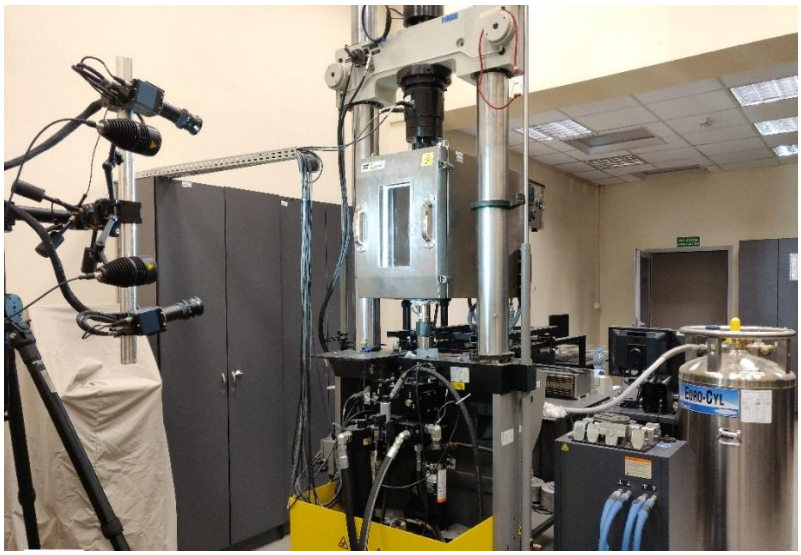


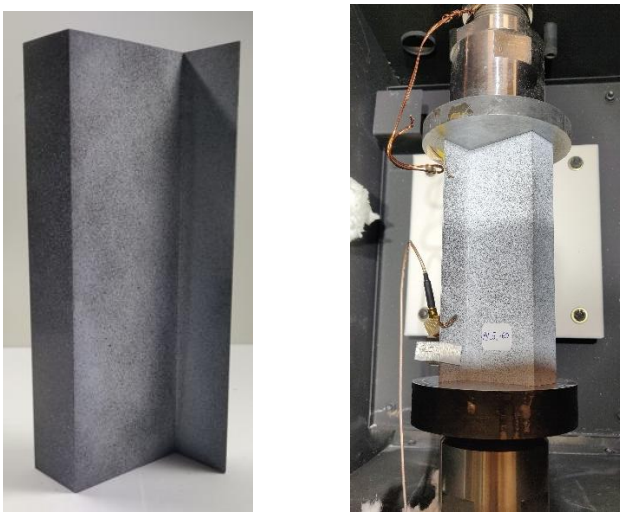
FIGURE 2.2. Experimental stand

2.3. ARAMIS system

The Aramis system belongs to the category of non-destructive methods and is used for optical analysis of displacements and deformations on the surface of a tested sample in three different directions during loading [46–48]. Its operation is based on the analysis of a series of digital images taken at regular time intervals by two precisely calibrated cameras positioned at an appropriate distance from the examined object. This enables the acquisition of detailed data on changes in geometry and strain distribution in real time. The Aramis system is distinguished

by its high resolution and measurement accuracy, making it particularly valuable in material research and mechanical engineering.

One of the key advantages of this method is its versatility—it allows for the analysis of both small samples under laboratory conditions and larger structural elements, regardless of their geometry or environmental conditions such as temperature and humidity. Moreover, this system enables a comprehensive assessment of material behavior under various loading conditions, which makes it widely applicable in civil engineering, aerospace, automotive industries, and biomaterial research.

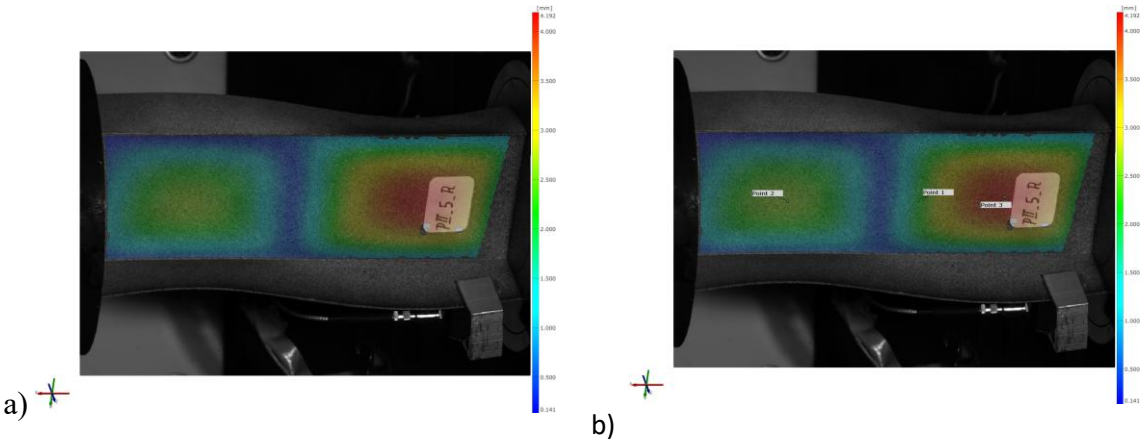


a) b)

FIGURE 2.3. A composite column prepared for testing: a) with an applied pattern, b) mounted in the machine grips.

The application of the contactless optical Aramis system requires a properly prepared measurement surface of the sample. For this purpose, the surface of the composite column was roughened and a pattern was applied—first, the sample surface was spray-coated with liquid chalk, and after drying, graphite was applied in a dotted pattern using the same method. This process resulted in a sample covered with a pattern consisting of a white background and contrasting black dots (Fig. 2.3.a).

The prepared sample was then placed in a temperature chamber and mounted in the grips of the MTS static testing machine (Fig. 2.3.b). Subsequently, the Aramis measurement system, consisting of two cameras, a converter, and a workstation with ZEISS software, was installed. The system was then calibrated using a reference plate with predefined reference points.



a) b)

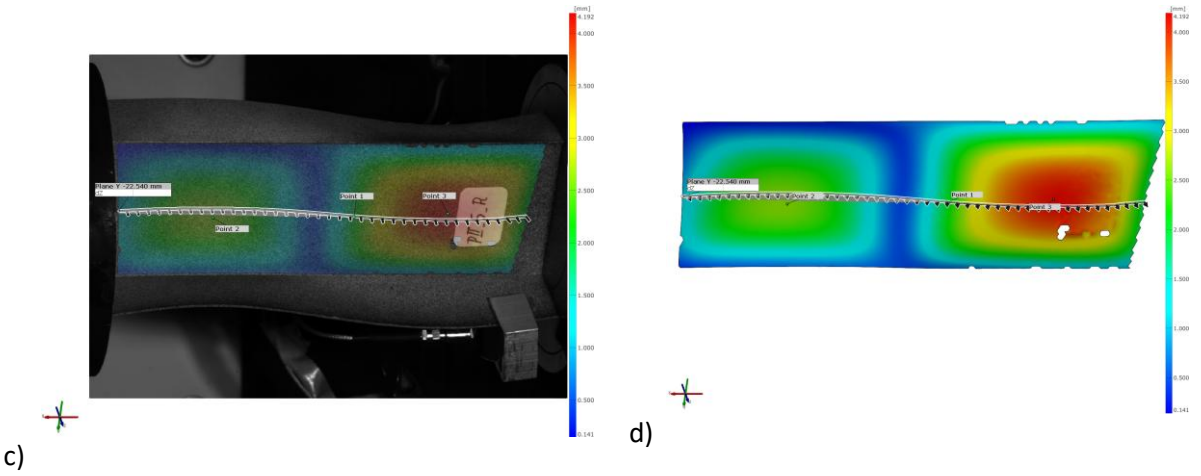


FIGURE 2.4. Test stand: a) surface component, b) identification of points at the locations of maximum web deflections, c) determination of the longitudinal cross-section plane of the column, d) displacement map of the average web deflections of the compressed column

The series of images captured using the contactless Aramis system was utilized for a comprehensive description of the deformation of the compressed column throughout the entire experimental test. The recorded experimental results, in the form of sample images and compressive force signals, were imported into the dedicated ZEISS software. Based on the sample's pattern, a surface component was generated (Fig. 2.4.a), which was then used to calculate displacements in three directions.

In the next step, three characteristic points were identified on the surface component of the column web at the locations of its maximum deflections (Fig. 2.4.b). To further analyze the deformation of the column, a cross-sectional analysis of the web was performed. The surface component was longitudinally sectioned along the XZ plane, and displacements in the Z vector direction (perpendicular to the web) were determined (Fig. 2.4.c). This allowed for the identification of the deflection trajectory of the compressed column within this plane.

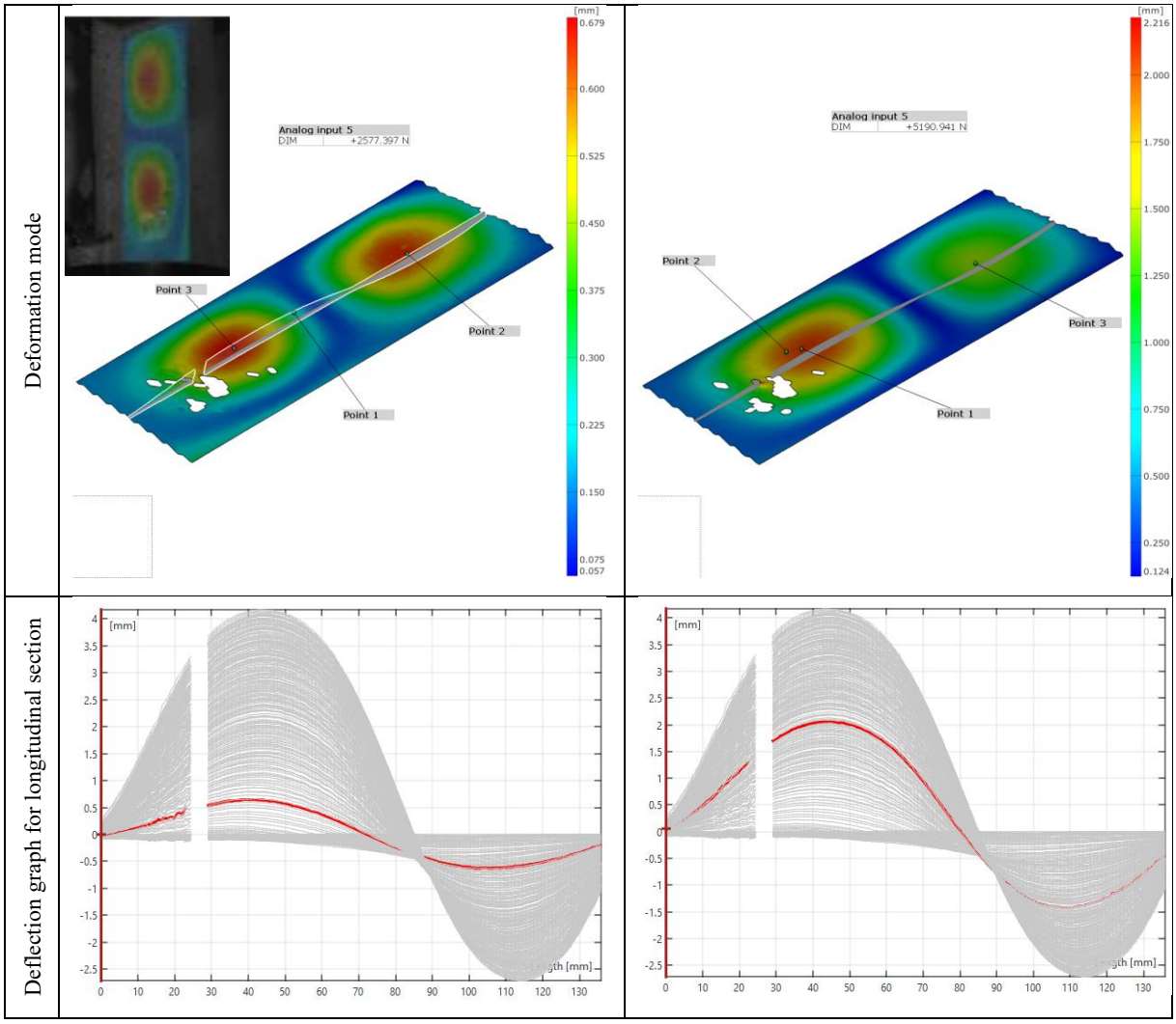
The application of ZEISS software for processing images captured by the Aramis system enables the development of a three-dimensional surface model. This model can be used to graphically display a displacement map of the compressed column (Fig. 2.4.d).

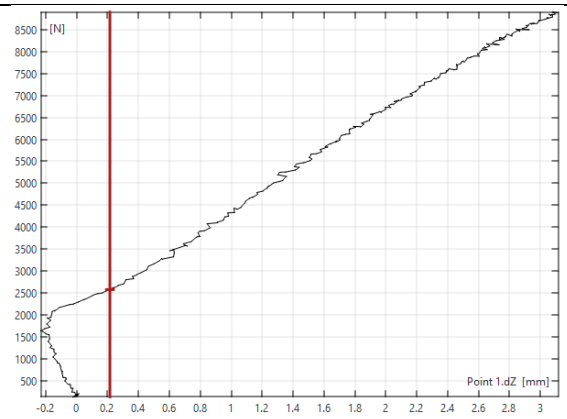
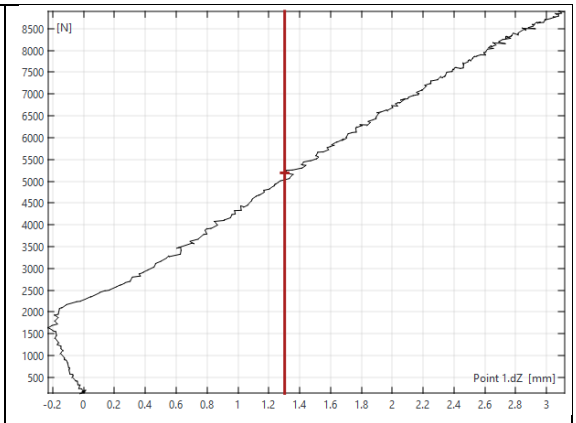
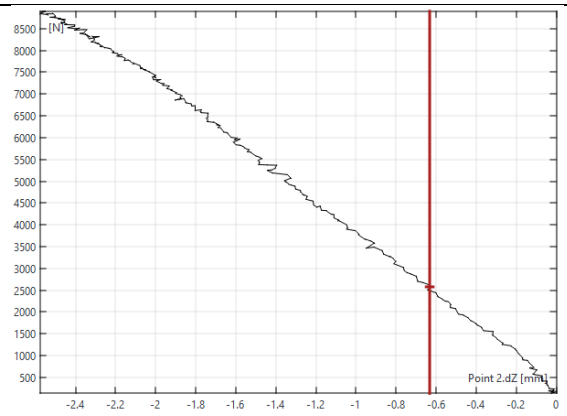
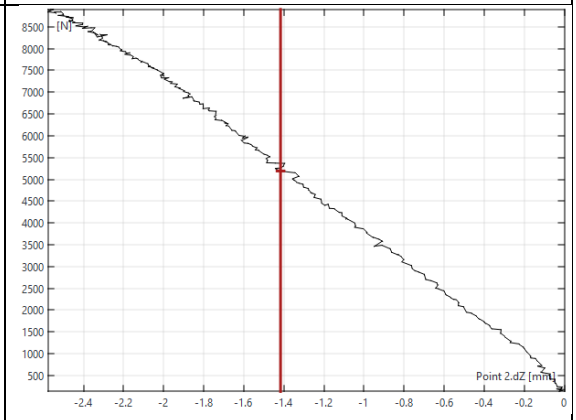
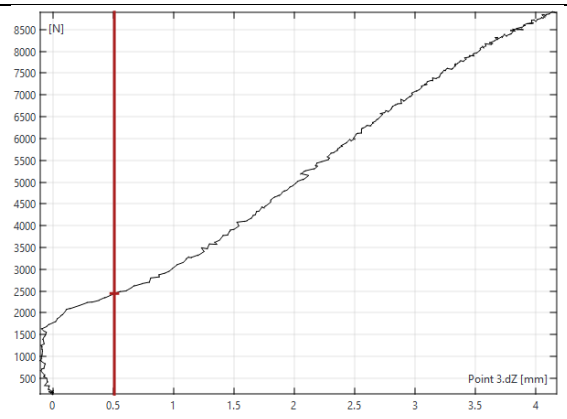
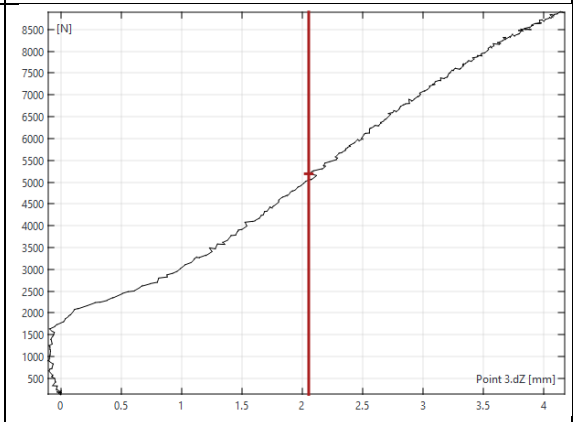
3. Results and discussion

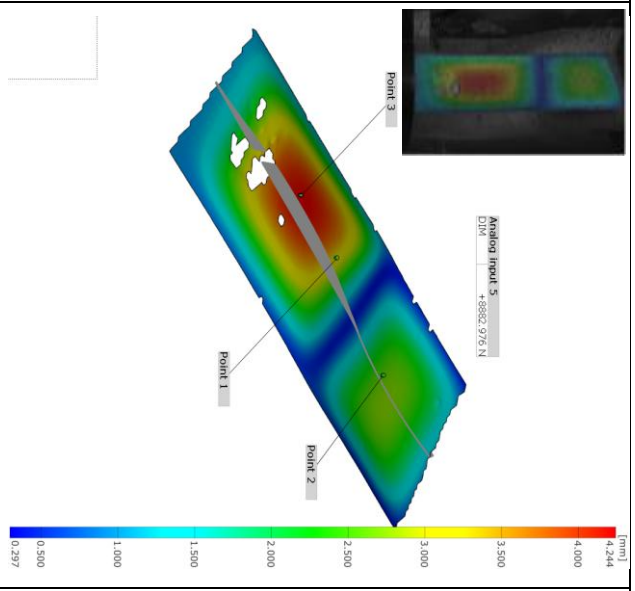
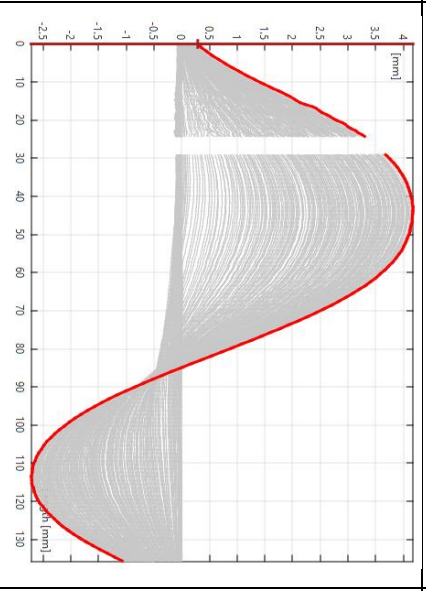
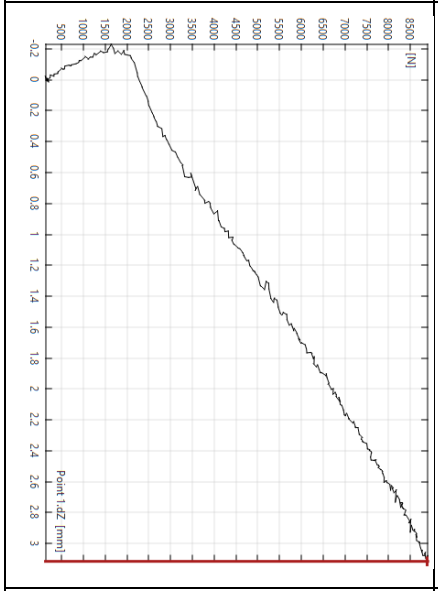
The analysis presents the effect of temperature on the behavior of composite profiles during compression (Fig. 3.1-3.5).The figures illustrate the buckling and deflection modes measured at selected measurement points for temperatures of -20°C, 20°C, 40°C, 60°C and 80°C. The deformation visualizations (bitmaps) depict structural changes as the load increases, highlighting areas of deformation concentration and its progression, the deflection graph specified in the longitudinal section of the column, and three equilibrium paths determined at the points of maximum transverse deflection (labeled as Point 1, Point 2, Point 3).

The load-displacement graphs indicate characteristic "jumps," which can be interpreted as sudden changes in buckling mode under increasing load (comparing the columns in each Fig.) and increasing temperature (comparing the Fig. 3.1-3.5). To sum up in Figure 3.6 presented mode shapes during the compression tests for all cases – 1st mode from the beginning of the test and the 2nd mode after transfer. For each temperature level, the figures combine: DIC

deformation maps, three reference points marked directly on the DIC fields, and corresponding equilibrium paths (load–displacement curves) plotted for each of these points. This approach enables a quantitative evaluation of mode transitions. Specifically, the three reference points indicated on the deformation maps correspond to distinct locations of curvature change within the profile. Their associated load–displacement plots clearly show: discontinuities in slope, sudden shifts in transverse displacement, and changes in the half-wave pattern, which together provide measurable criteria identifying the exact moment of mode jumping. These discontinuities are visible as sharp deviations in the plotted equilibrium paths in Figs. 3.1–3.5 for all temperatures.



Load-displacement paths for Point 1		
Load-displacement paths for Point 2		
Load-displacement paths for Point 3		
	a)	b)

Deformation mode	Deflection graph for longitudinal section	Load-displacement paths for Point 1
		

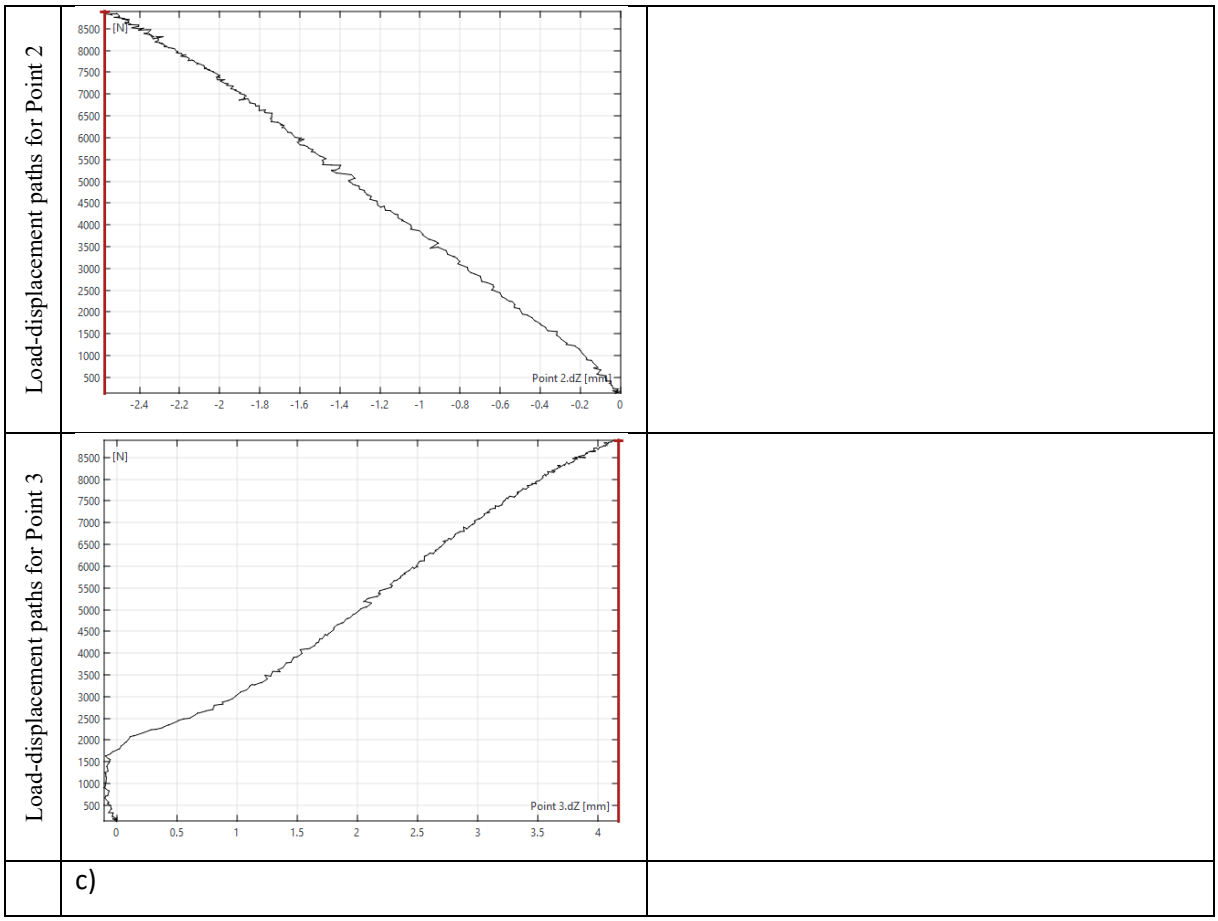
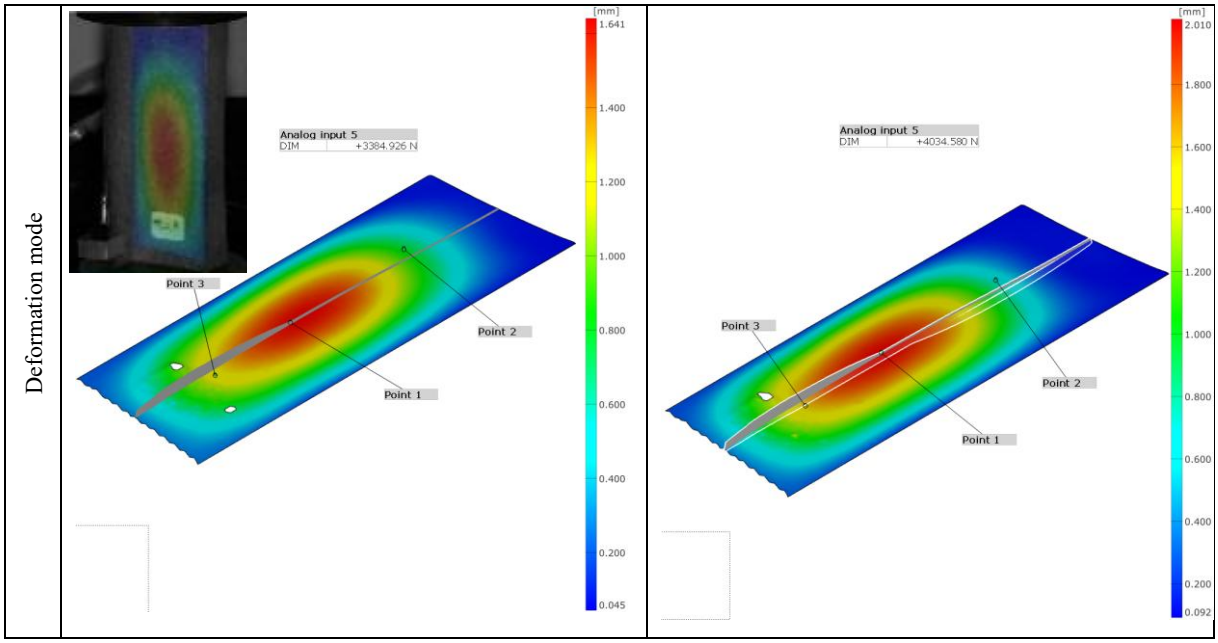
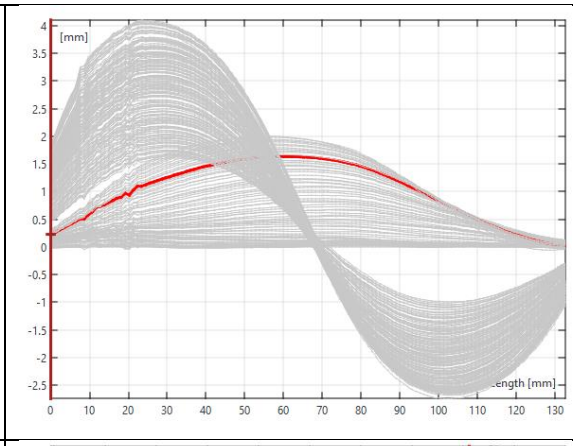
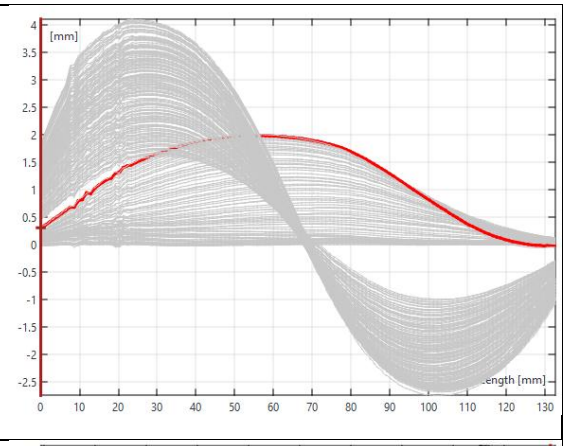
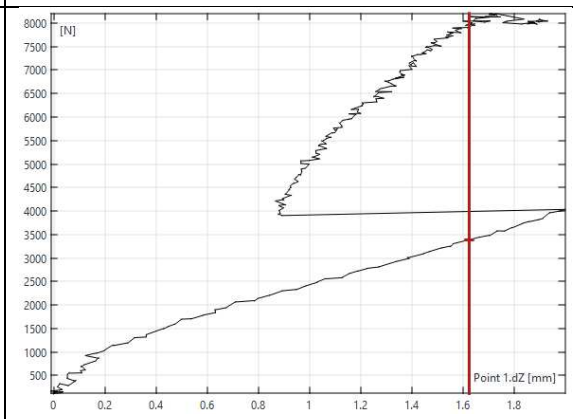
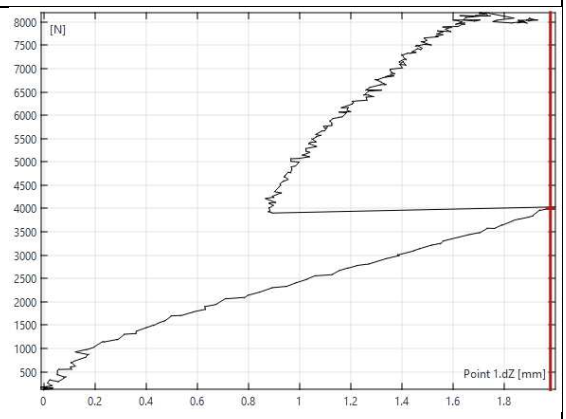
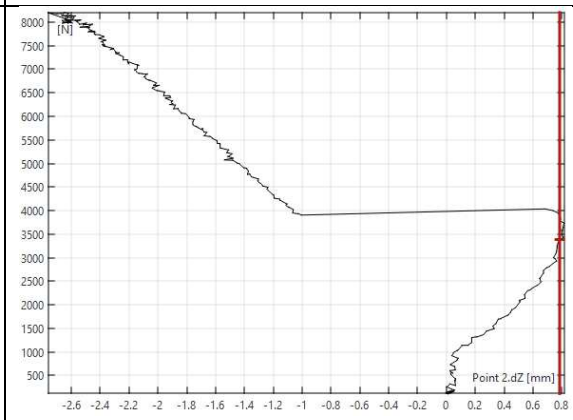
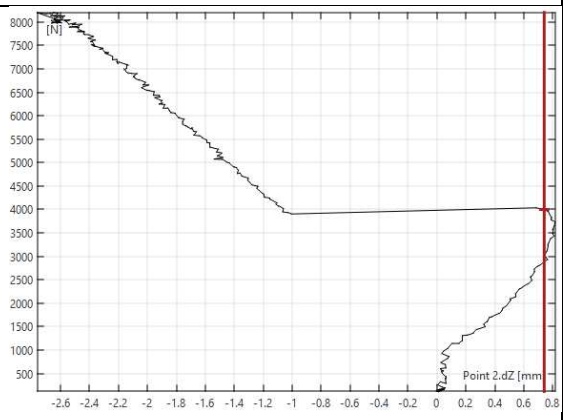
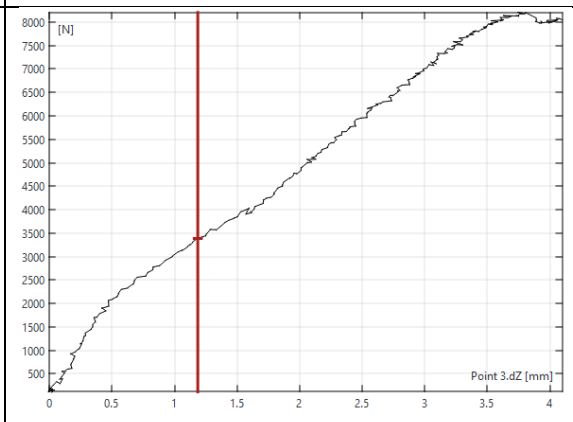
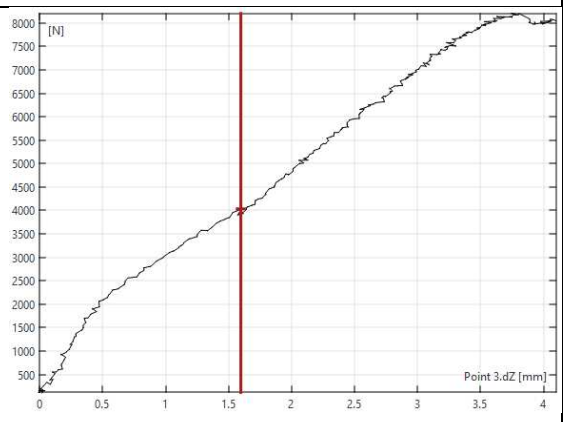
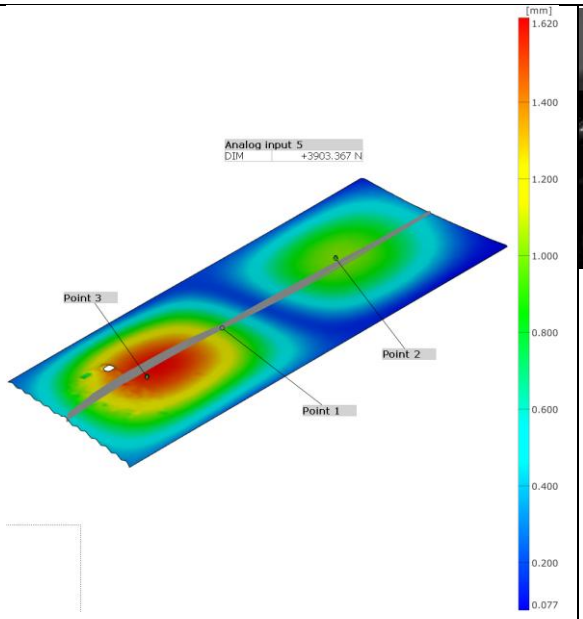
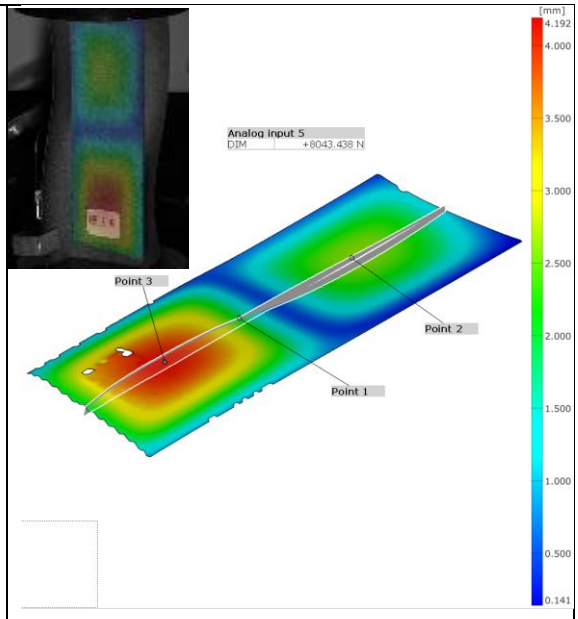
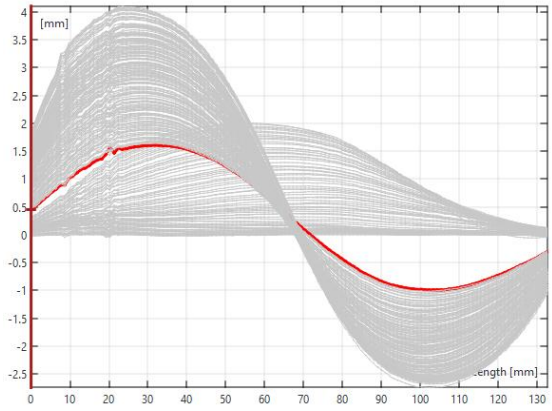
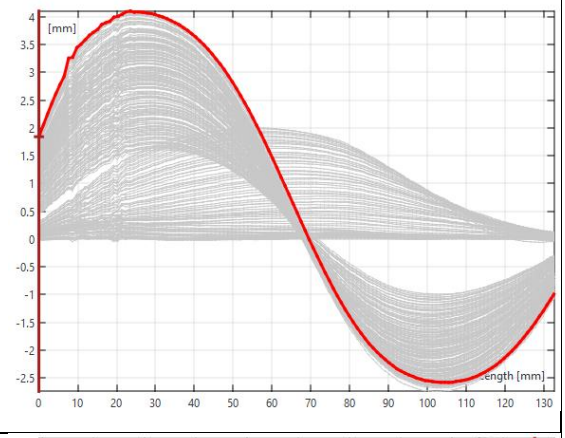
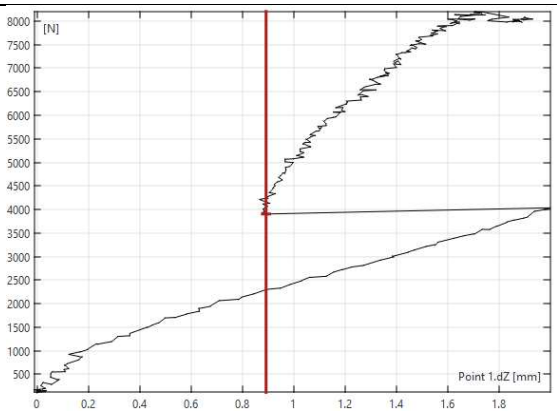
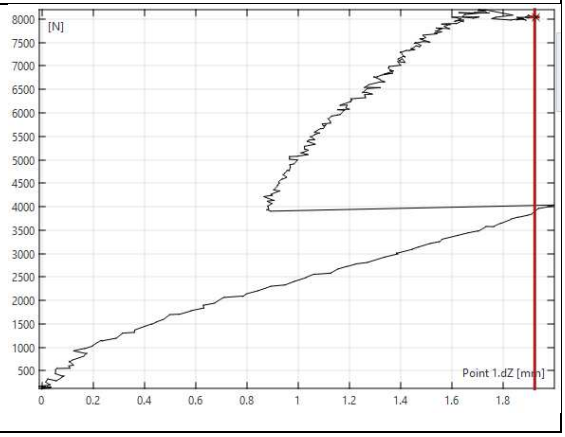


FIGURE 3.1. Advanced analysis of the composite profile under compression at -20ºC: a) buckling, b) postcritical deformation, c) limit deformation



Deflection graph for longitudinal section		
Load-displacement paths for Point 1		
Load-displacement paths for Point 2		
Load-displacement paths for Point 3		
	a)	b)

Deformation mode		
Deflection graph for longitudinal section		
Load-displacement paths for Point 1		

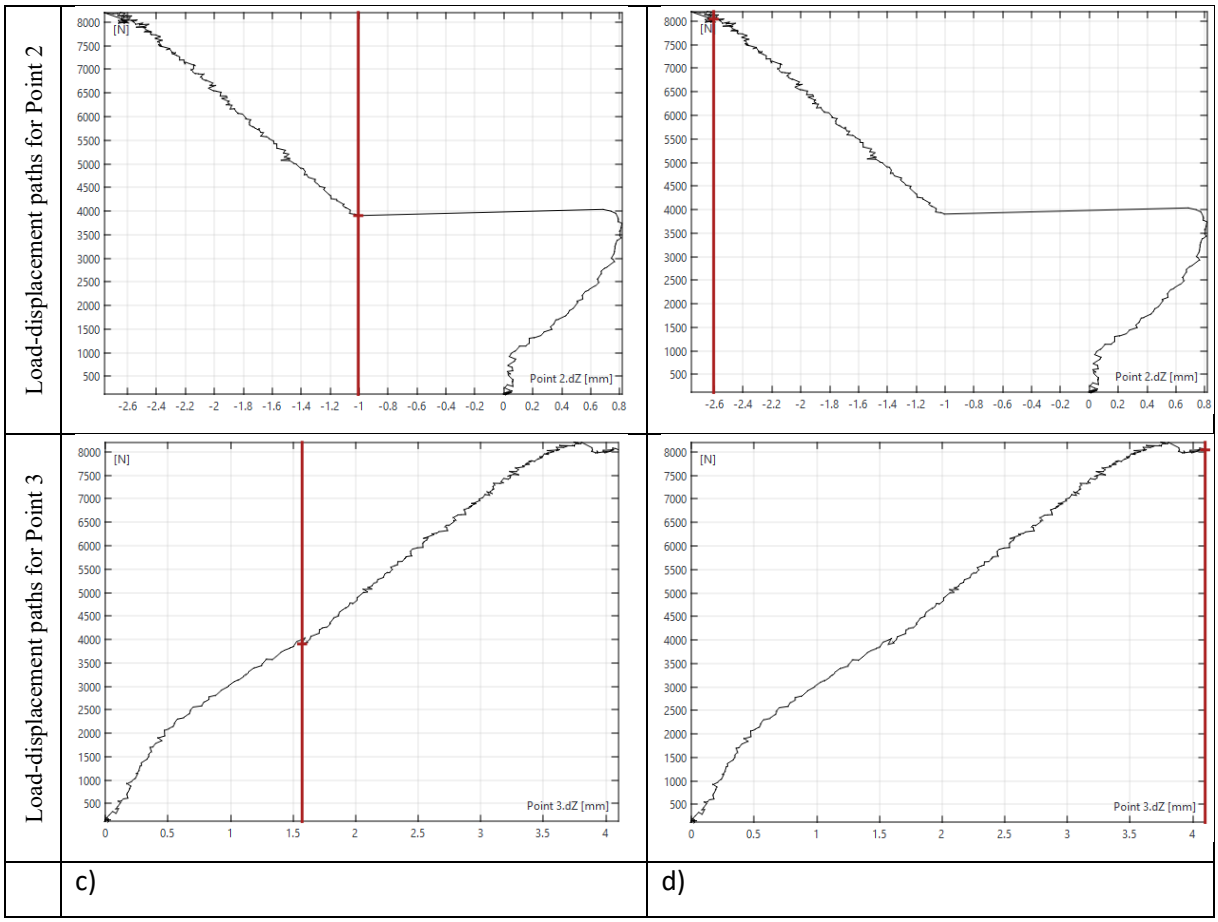
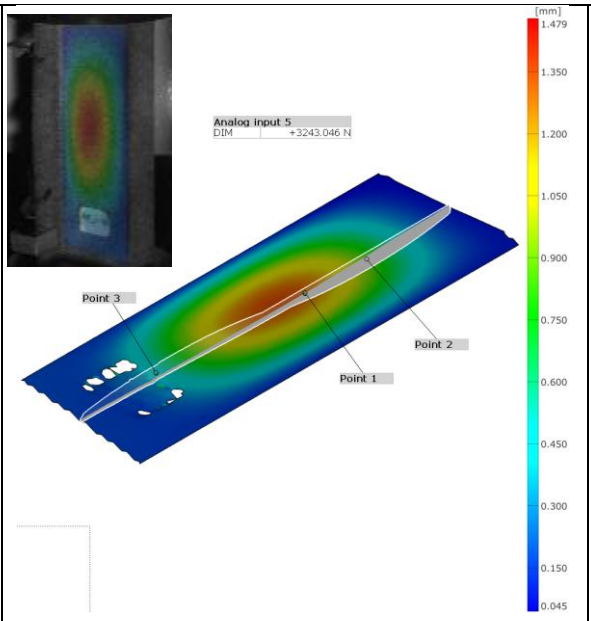
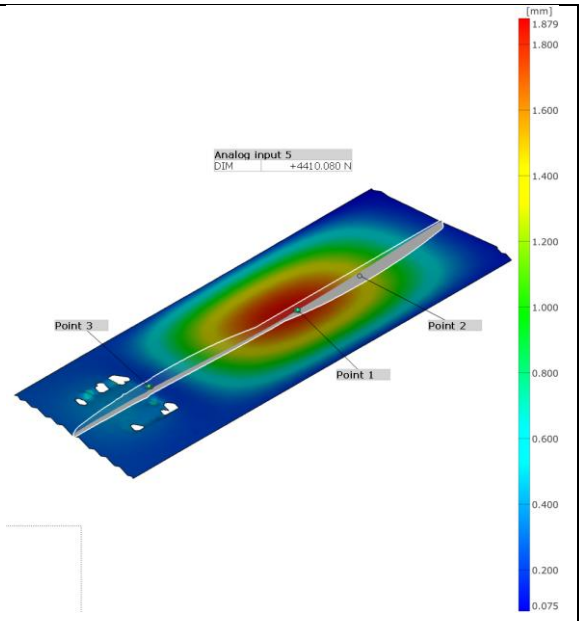
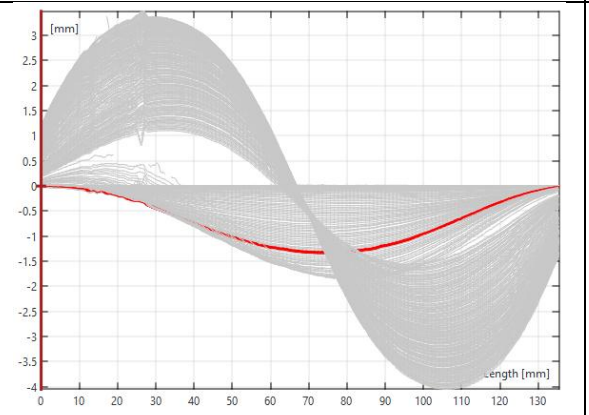
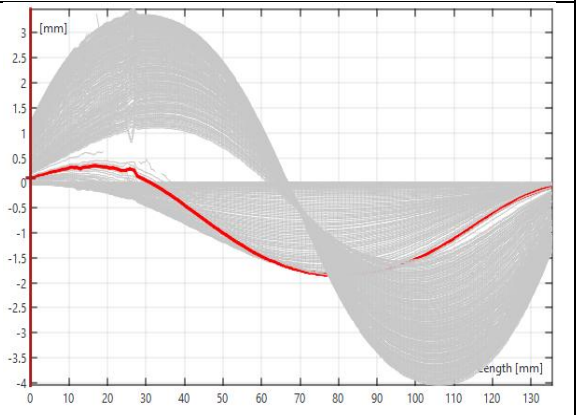
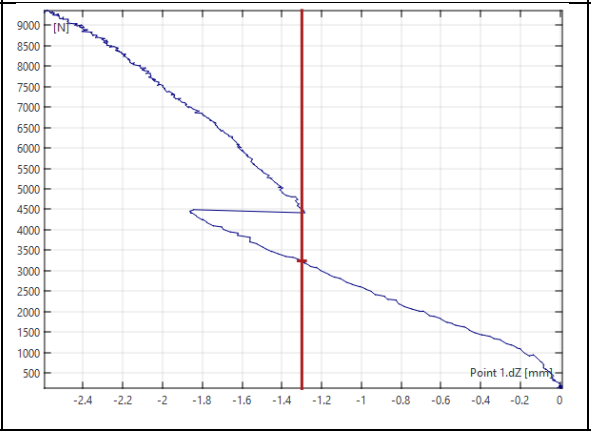
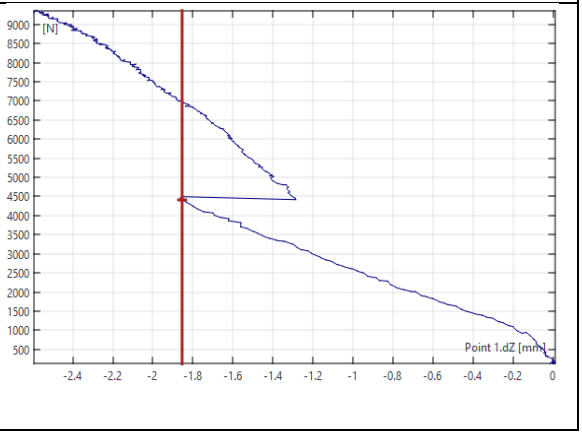
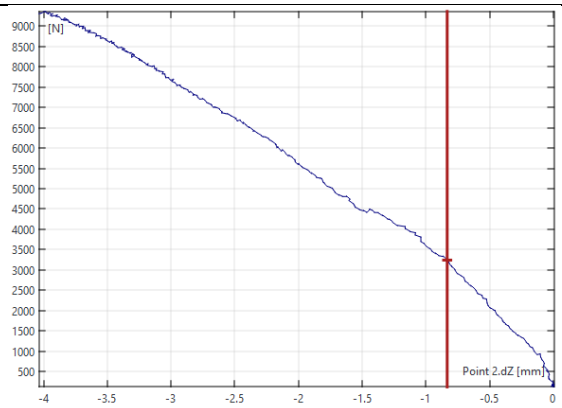
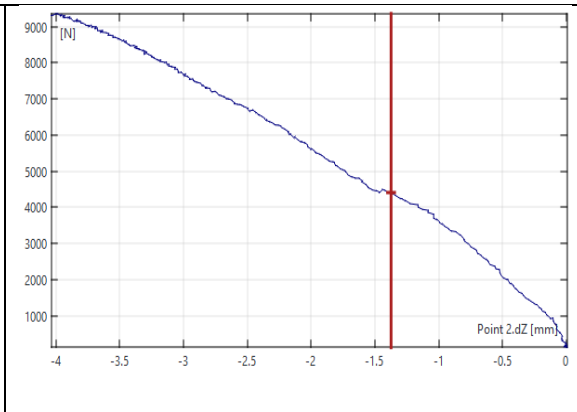
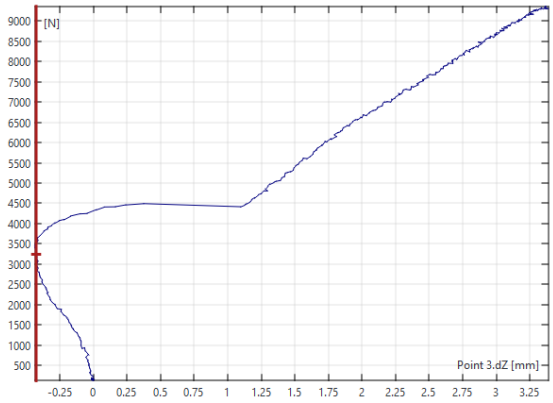
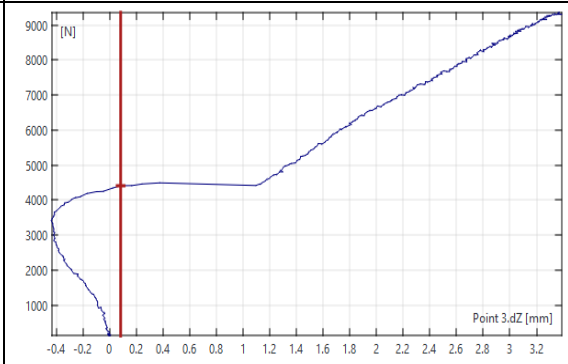
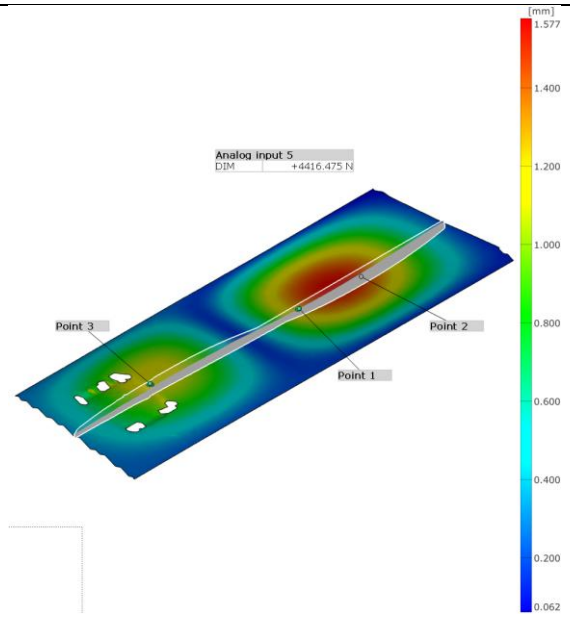
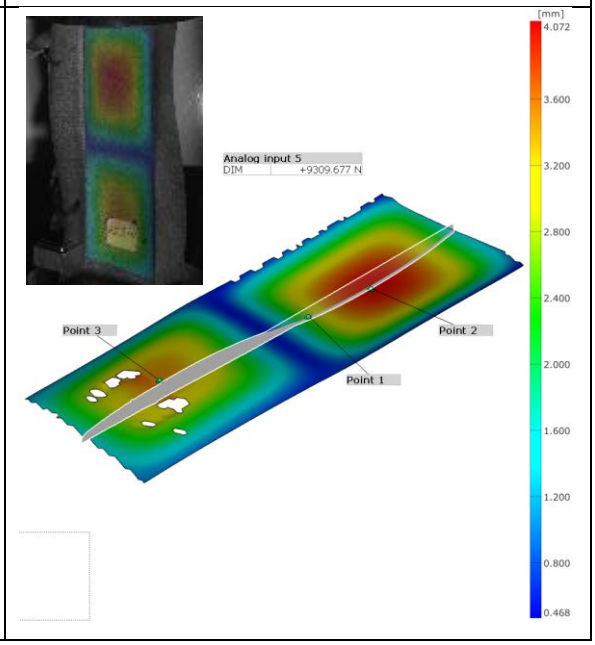


FIGURE 3.2. Advanced analysis of the composite profile under compression at 20ºC: a) buckling, b) postbuckling deformation, c) postcritical deformation , d) limit deformation

Based on the comparison of results for temperatures of -20°C and 20°C, significant differences in the buckling mode of compressed composite profiles can be observed. At -20°C, the initial deformation consists of two half-waves, indicating a more complex buckling mode typical for materials with increased stiffness at low temperatures. As the temperature increases to 20°C, the initial buckling mode changes, starting with a single half-wave before transitioning into a more stable mode with two half-waves.

Deformation mode		
Deflection graph for longitudinal section		
Load-displacement paths for Point 1		

Load-displacement paths for Point 2		
Load-displacement paths for Point 3		
	a)	b)
Deformation mode		

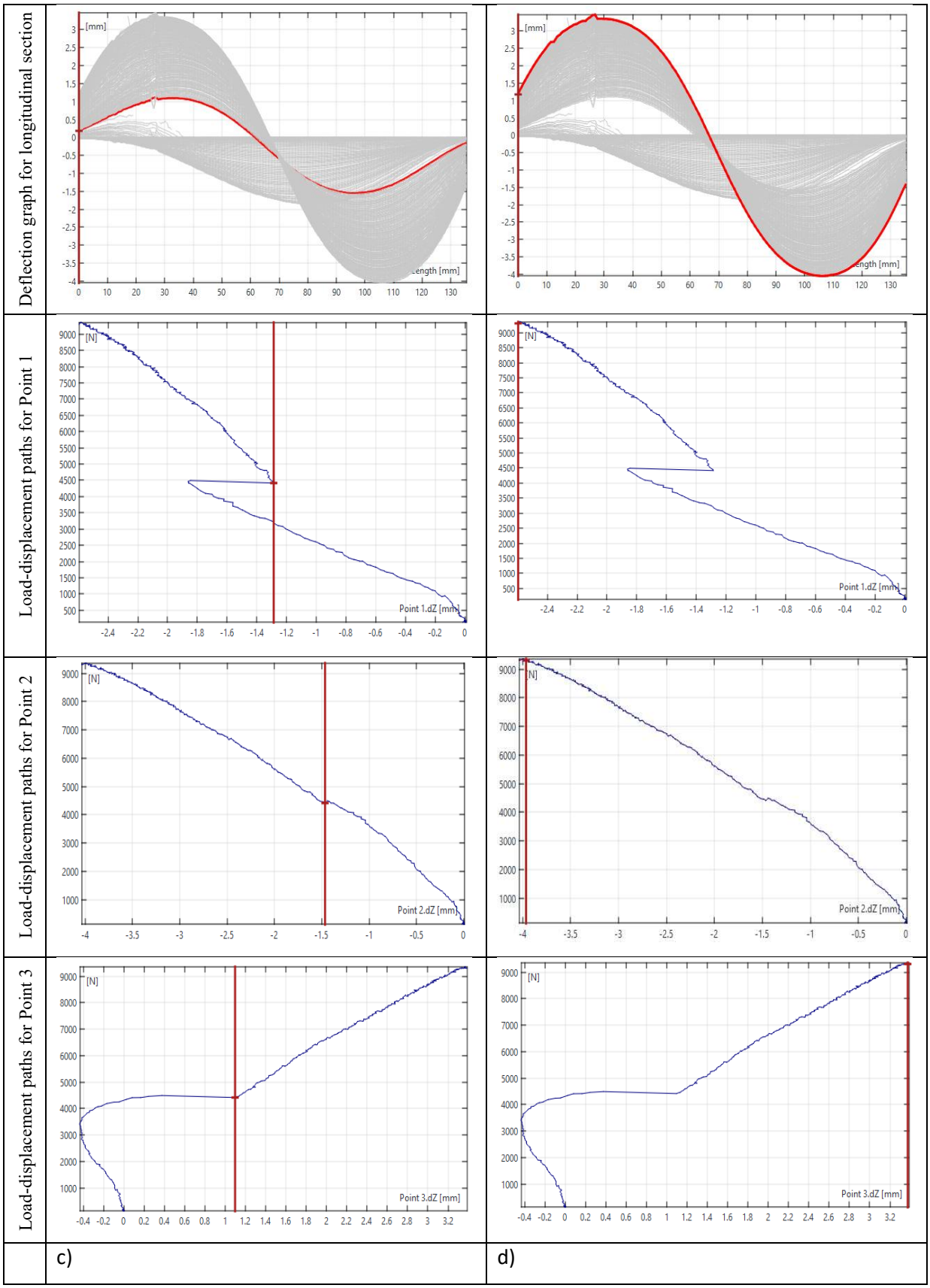
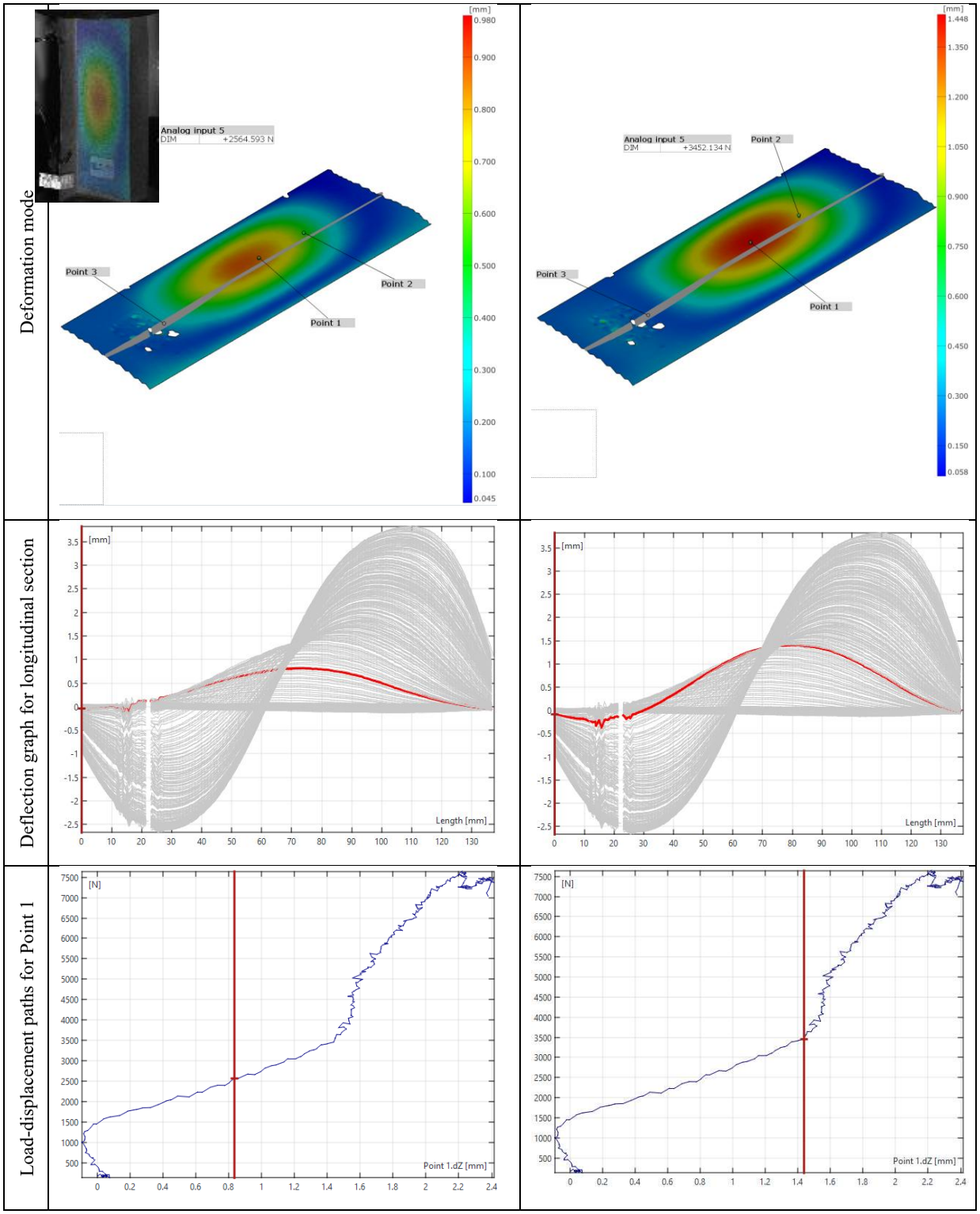
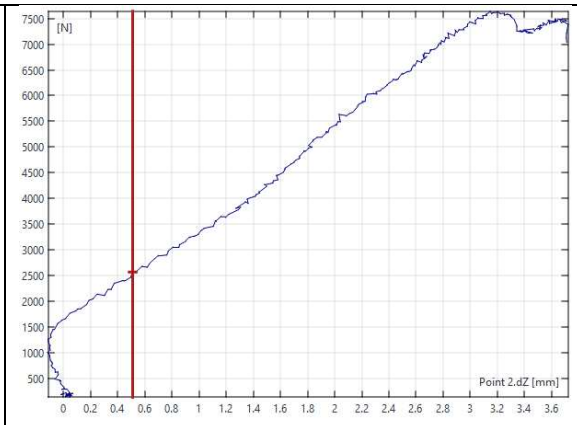
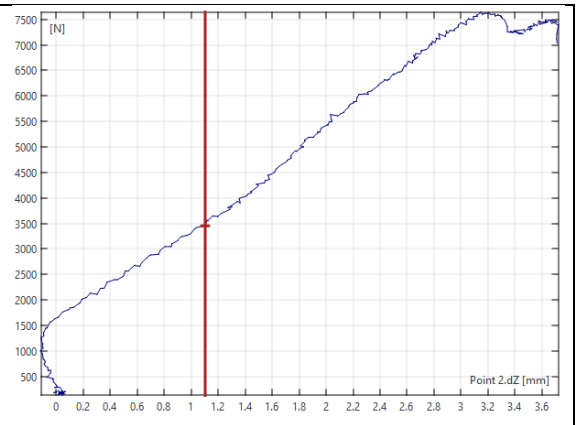
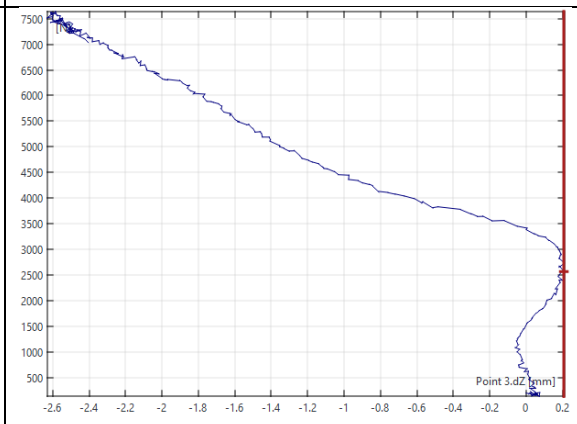
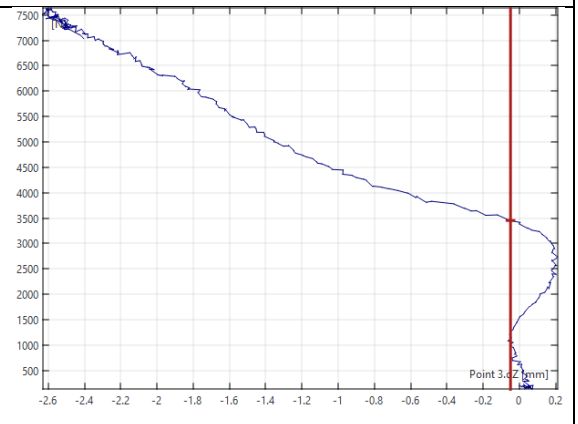
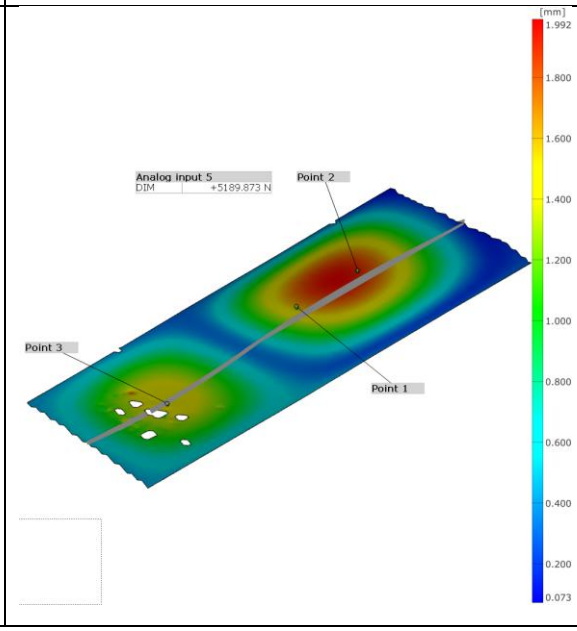
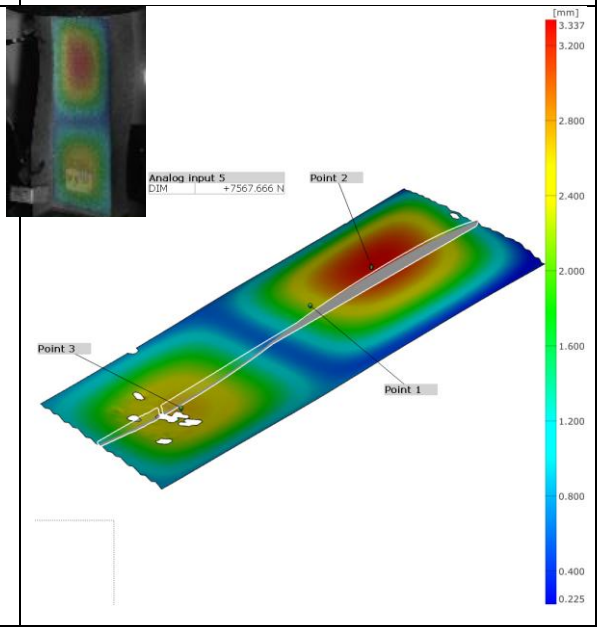


FIGURE 3.3. Advanced analysis of the composite profile under compression at 40ºC: a) buckling, b) postbuckling deformation, c) postcritical deformation , d) limit deformation


Deformation mode
Analog input 5
DIM +2564.593 N
[mm]
0.980
0.900
0.800
0.700
0.600
0.500
0.400
0.300
0.200
0.100
0.045
Point 3
Point 2
Point 1
Analog input 5
DIM +3452.134 N
[mm]
1.448
1.350
1.200
1.050
0.900
0.750
0.600
0.450
0.300
0.150
0.058
Point 2
Point 3
Point 1
Deflection graph for longitudinal section
[mm]
Length [mm]
Load-displacement paths for Point 1
[N]
Point 1.dZ [mm]

Load-displacement paths for Point 2		
Load-displacement paths for Point 3		
	a)	b)
Deformation mode		

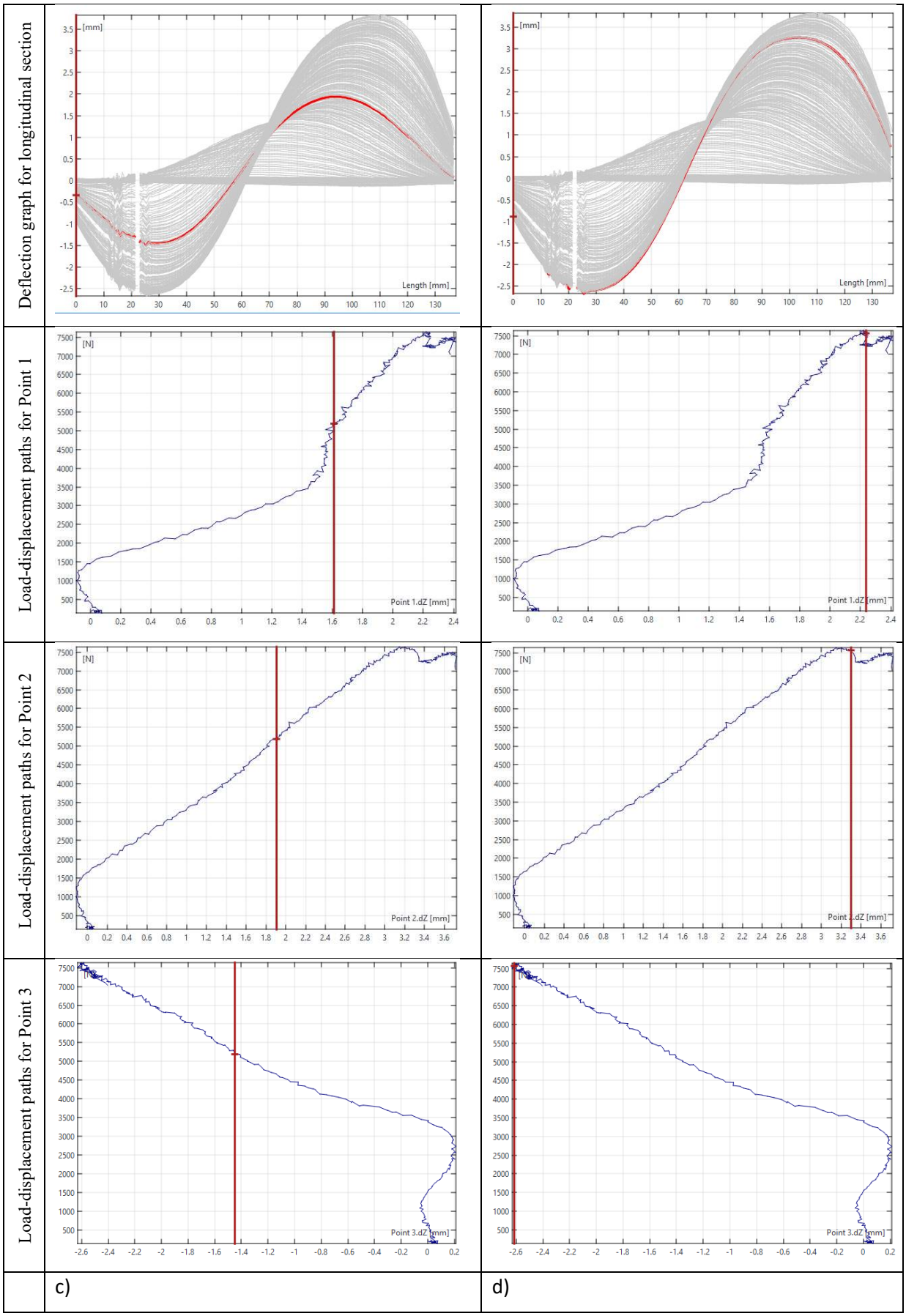
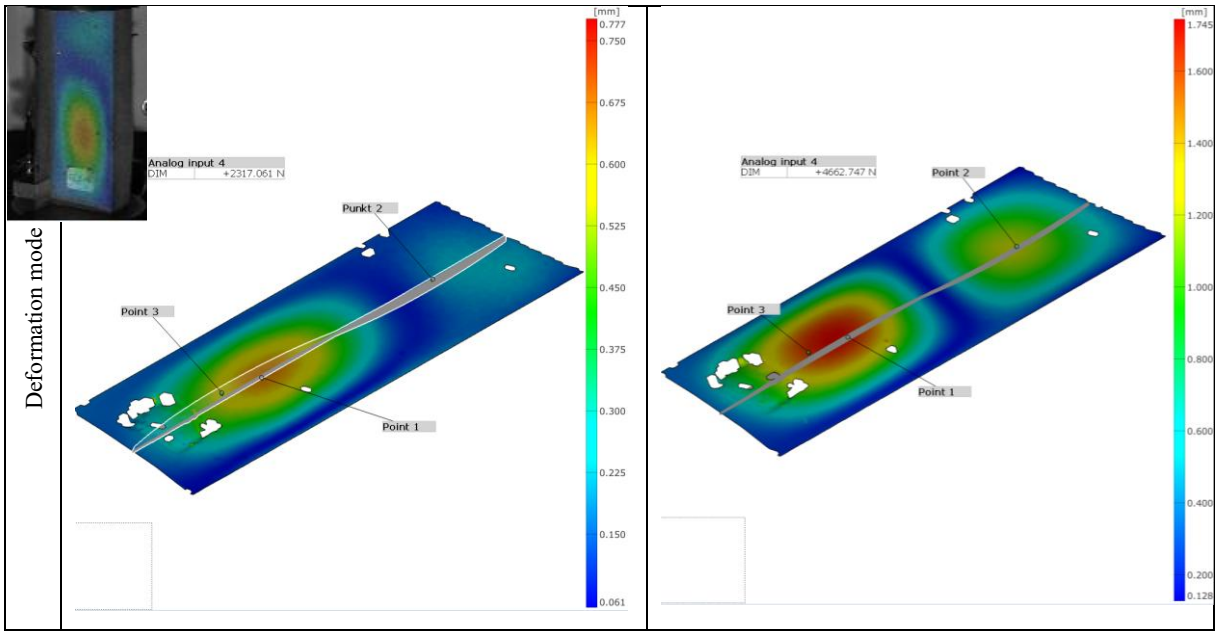


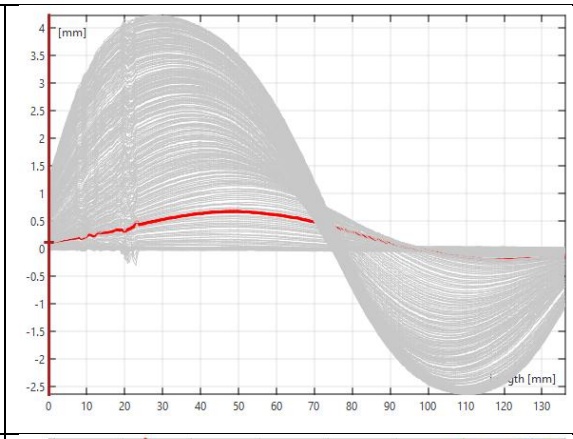
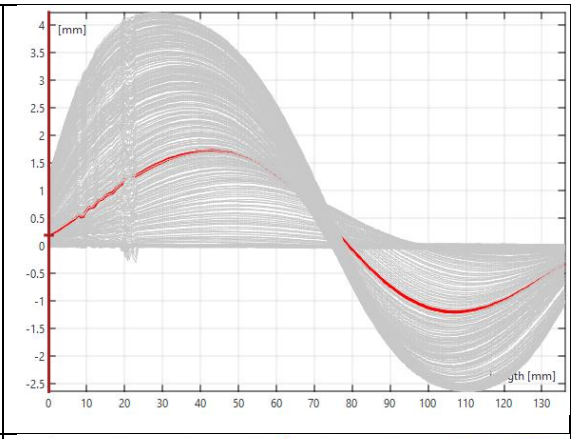
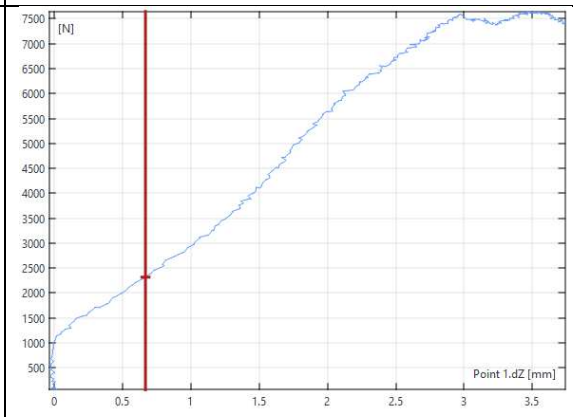
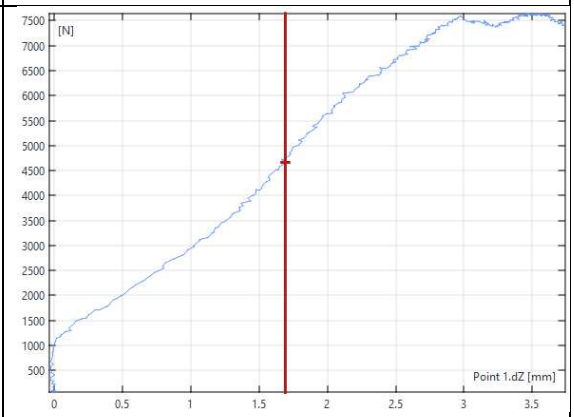
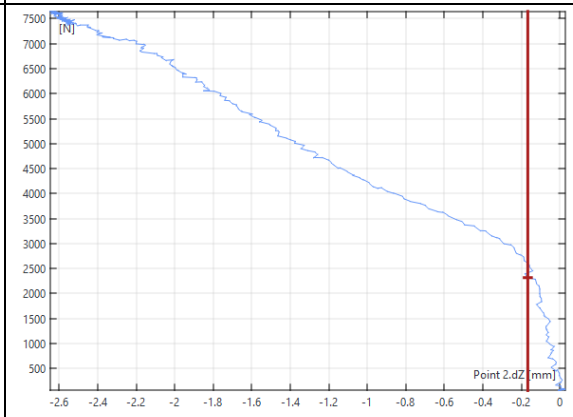
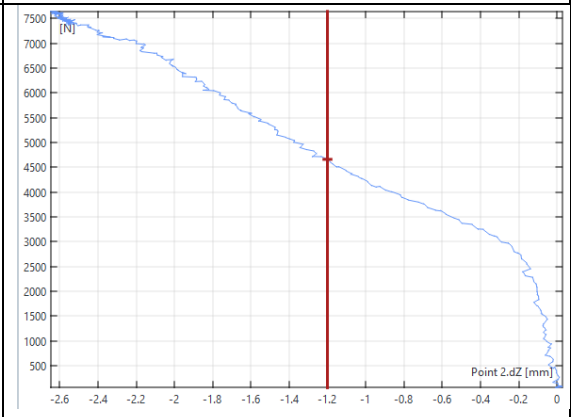
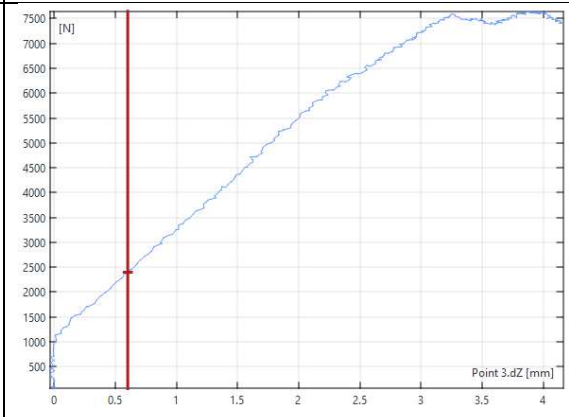
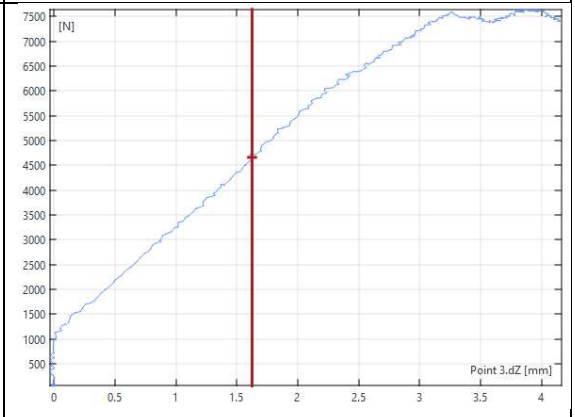
FIGURE 3.4. Advanced analysis of the composite profile under compression at 60ºC: a) buckling, b) postbuckling deformation, c) postcritical deformation , d) limit deformation

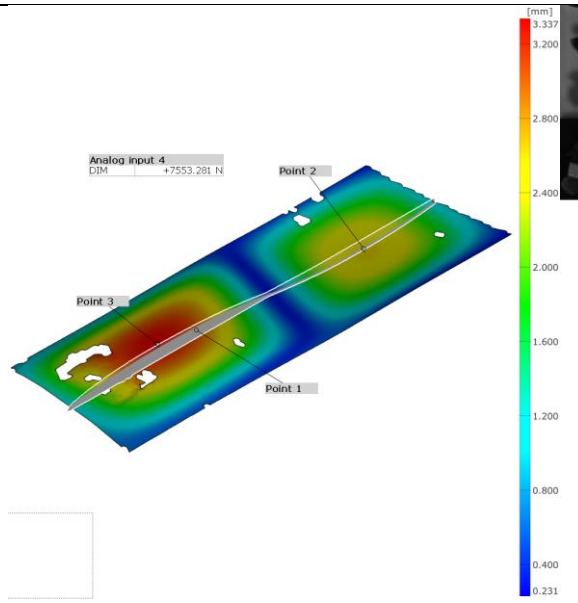
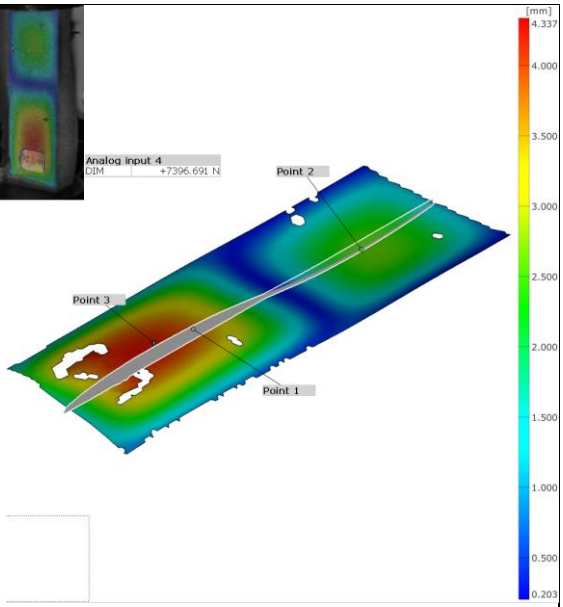
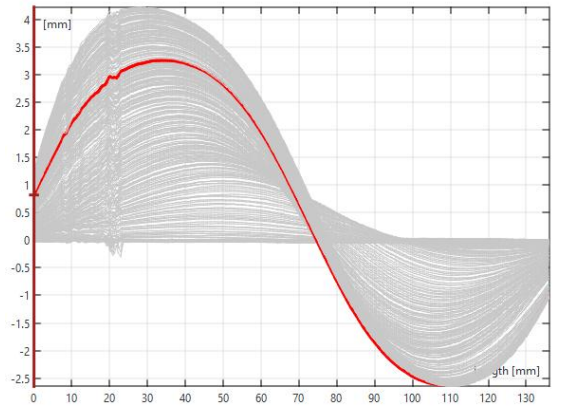
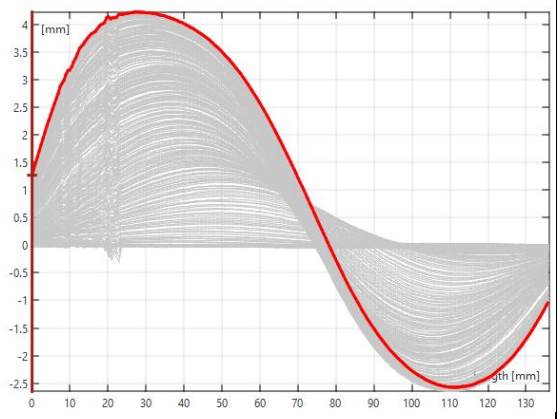
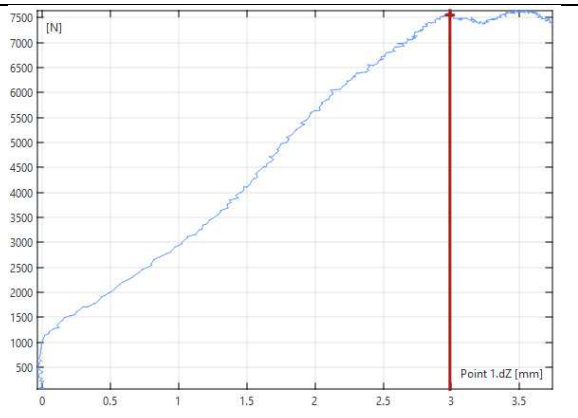
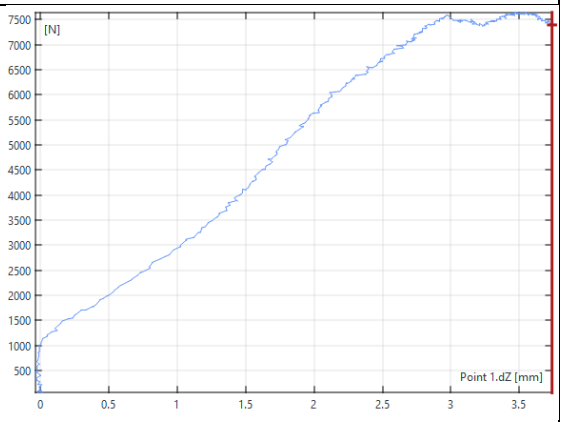
Based on the results for temperatures of 40°C and 60°C, further changes in the buckling mode can be observed compared to -20°C and 20°C. The analysis clearly demonstrates the influence of temperature on deformation mechanics, leading to significant structural weakening of composite profiles and modifications in buckling behavior.

At 60°C, buckling initially occurs with a single half-wave and remains in this form for an extended period before transitioning to a two-half-wave mode under increased loading. This contrasts with lower temperatures, where the buckling mode transition occurred more rapidly and distinctly. Displacement graphs for Points 1, 2, and 3 indicate smoother and less abrupt changes; however, at critical loading, a significant reduction in load-bearing capacity is observed, confirming the degradation of mechanical properties.

This transition effect results from the deterioration of composite mechanical properties at elevated temperatures, reducing stiffness and altering the deformation growth pattern. As noted in the literature, at higher temperatures, composite materials experience mechanical degradation, leading to a decrease in critical buckling load and a change in deformation mode [27]. This phenomenon has also been described by Hu et al. [49], where temperature variations cause a shift from symmetric global deformations to localized ones, explaining the observed differences in buckling behavior.



Deflection graph for longitudinal section		
Load-displacement paths for Point 1		
Load-displacement paths for Point 2		
Load-displacement paths for Point 3		
	a)	b)

Deformation mode		
Deflection graph for longitudinal section		
Load-displacement paths for Point 1		

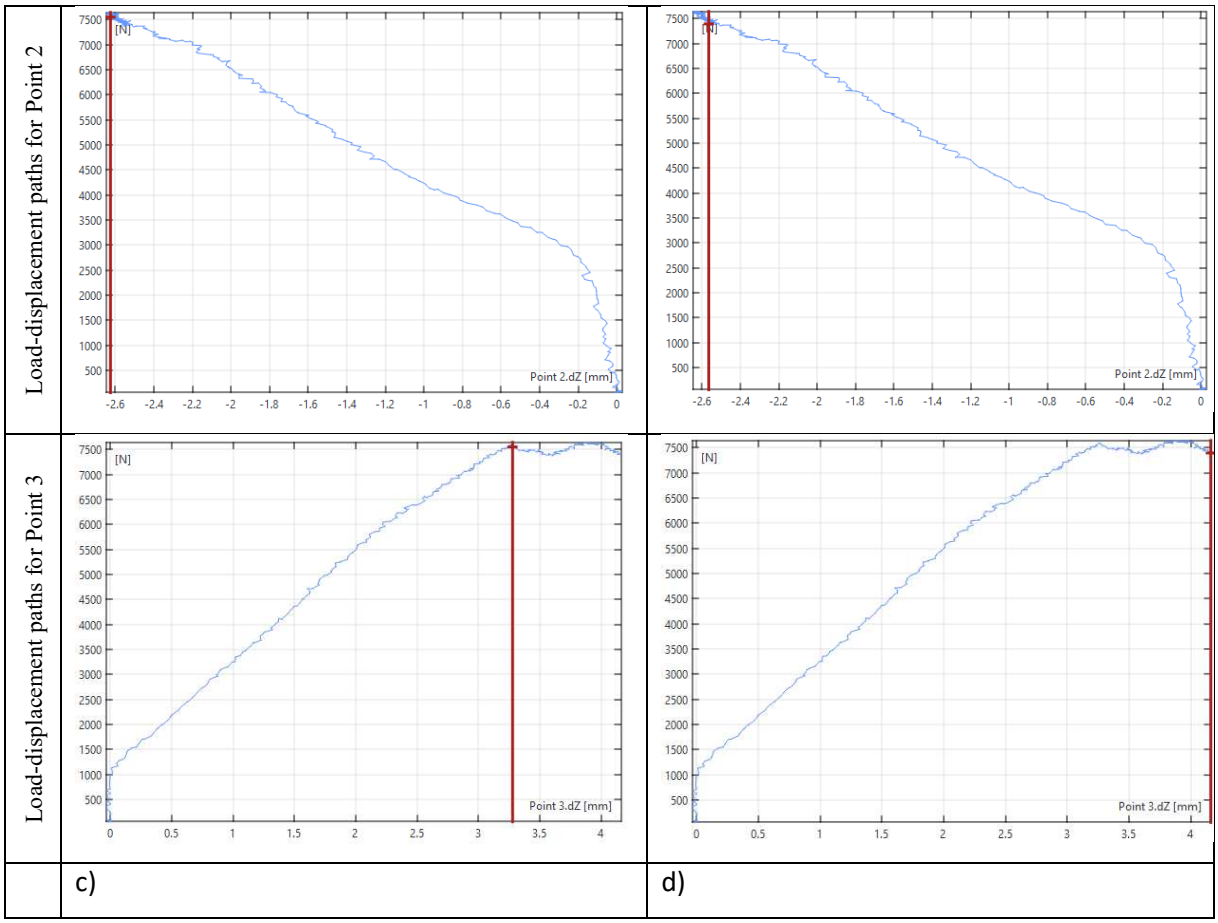


FIGURE 3.5. Advanced analysis of the composite profile under compression at 80ºC: a) buckling, b) postbuckling deformation, c) postcritical deformation , d) limit deformation

At 80°C, the initial buckling mode is characterized by a single half-wave, which rapidly transitions into a more complex two-half-wave pattern. The composite profile at this temperature exhibits lower resistance compared to 60°C, as evident in the displacement graphs for Points 1, 2, and 3. The load-displacement characteristics indicate a significant reduction in the critical load, confirming the structural degradation of the material at this temperature. The graphs suggest increased asymmetry in deformation and greater sensitivity to temperature variations.

It is important to emphasize that the mode transitions identified in Figs. 3.1–3.5 are not based solely on qualitative DIC visualisation. The three reference points marked on each deformation map provide quantitative evidence of sudden shifts in displacement behaviour. The load–displacement curves associated with Points 1–3 reveal slope discontinuities and inflection points that correspond exactly to the observed redistribution of half-waves. Additionally, the longitudinal DIC cross-sections (second row in each figure) show abrupt changes in curvature, which serve as a measurable indicator of mode jumping. These combined observations confirm that the transition between buckling modes can be objectively identified and quantified.

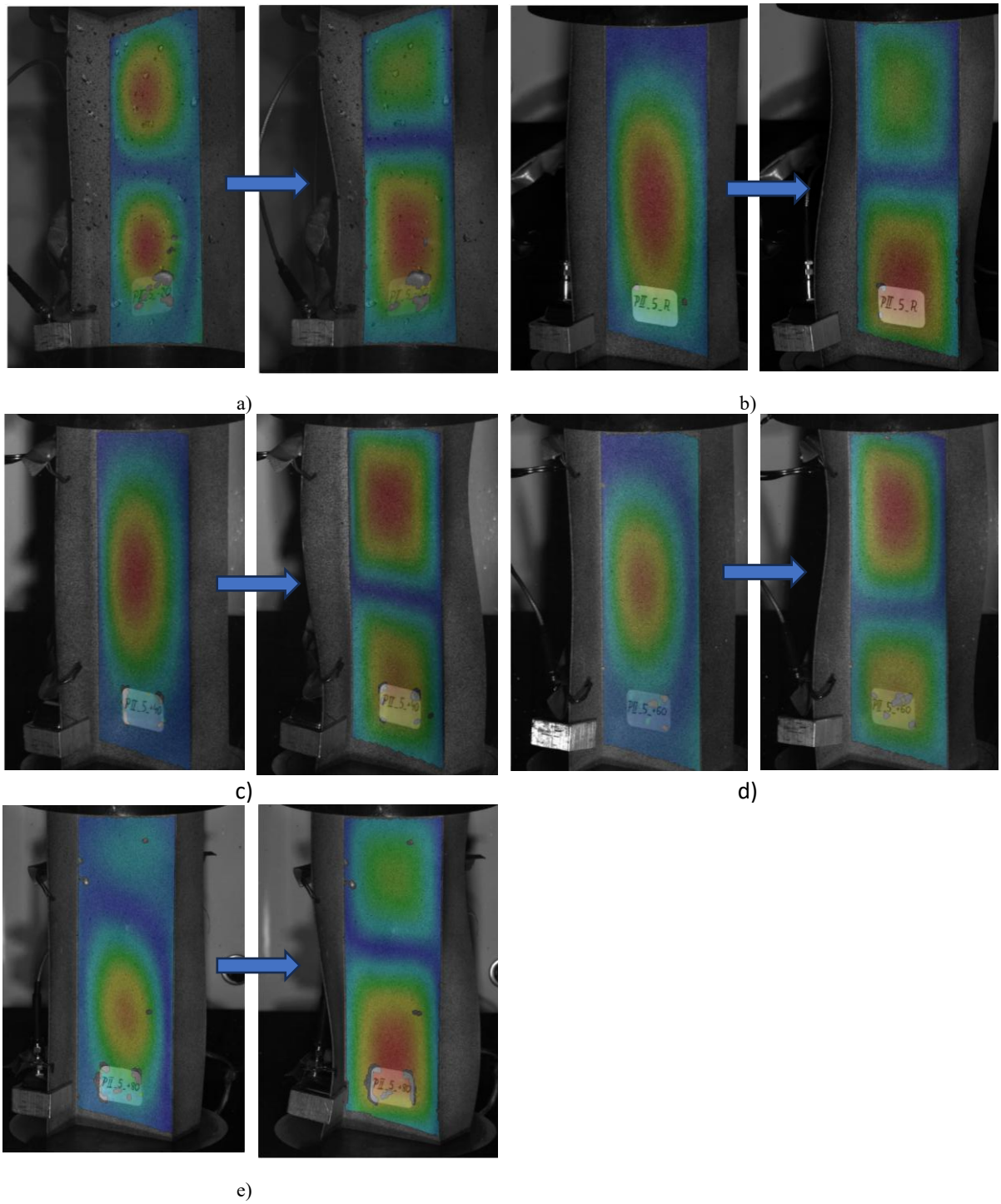


FIGURE 3.6. Mode shapes during axial compression for different temperatures: a) -20°C, b) 20°C, c) 40°C, d) 80°C, e) 80°C

Moreover, all Figures confirm how important is that the selection of the point for displacement analysis, because as we can observe, we can obtain different characteristics from different chosen half-waves.

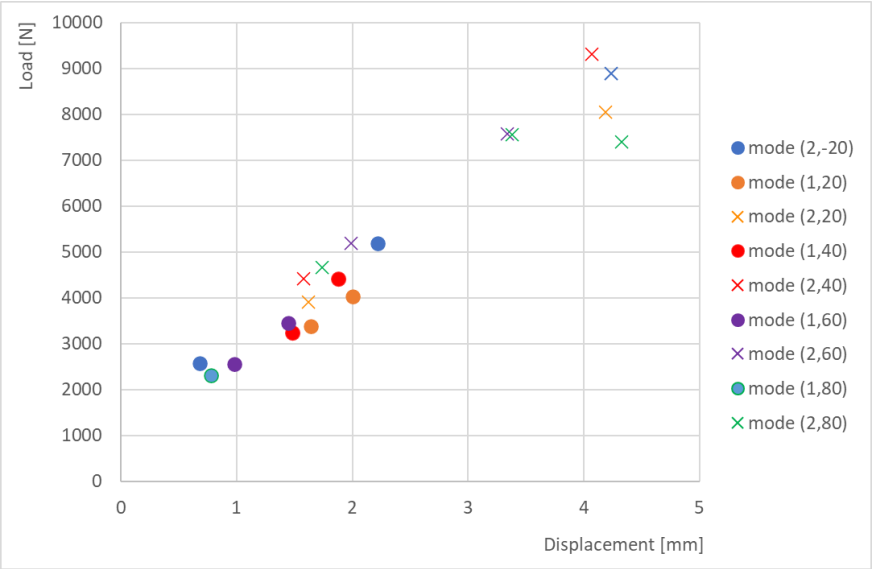


FIGURE 3.7. Analysis of buckling mode for different temperatures

Additionally, Figure 3.7 illustrates the variation of buckling modes for different temperatures, represented through the load-displacement relationship. The data clearly indicate that the buckling response of the material evolves with temperature changes, affecting both the critical load and the mode shape. The plotted points show a transition between buckling modes as the temperature changes, suggesting a temperature-dependent behaviour in the structural response. The maximum load-carrying capacity fluctuates across different temperatures, with higher temperatures generally reducing the critical load due to softening of the material of matrix, while lower temperatures increase stiffness and buckling resistance. Buckling modes at higher temperatures tend to reach larger displacements before failure, reflecting a more ductile response, whereas at lower temperatures, the response is stiffer and more brittle-like, resulting in earlier buckling. Each mode is distinct in the legend, with the notation indicating the associated temperature (e.g., 2, 20; 2, 40; 2, 80), which helps track how the response shifts with thermal variation.

This figure provides valuable insight into how thermal conditions affect the stability and post-buckling behaviour of composite materials, emphasizing the importance of temperature considerations in design and reliability analysis.

In summary, the greatest reduction in load-bearing capacity and buckling strength occurs at 80°C, indicating that the material loses a significant portion of its original compressive strength at this temperature. Similar to 60°C, buckling initially begins with a single half-wave, but the transition to two half-waves happens more quickly and less stably, suggesting greater structural weakening. It can be inferred that high temperatures cause more dispersed and uneven

deformations, increasing the risk of localized damage. This process is typical for composites at elevated temperatures, where the matrix loses its mechanical properties.

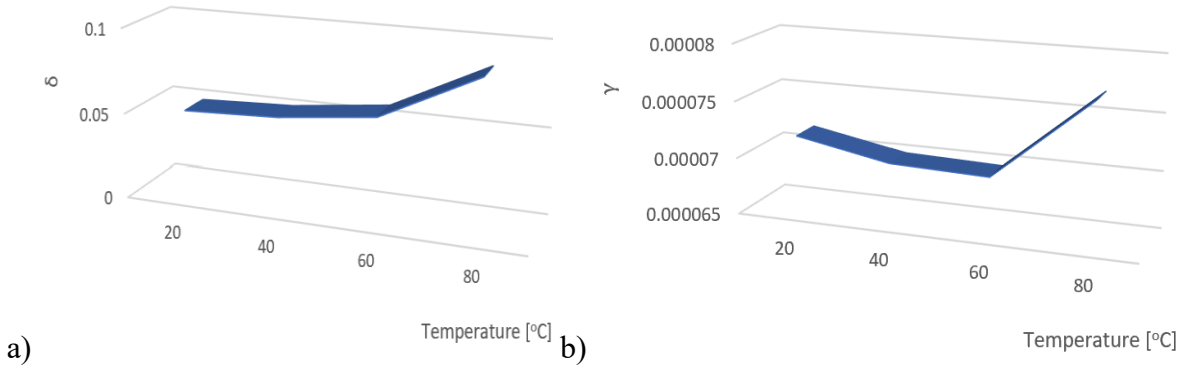
Nemeth's studies highlight the significant influence of bending–twisting coupling—represented by the (D_{16} and D_{26} terms) —on the buckling behaviour of composite laminates [50]. An increased level of bend–twist anisotropy, particularly associated with elevated (i.e. D_{26}) values, results in the emergence of more inclined, spiral-shaped buckling modes.

To quantify the degree of anisotropy and assess its impact on buckling, Nemeth proposed an flexural anisotropy factors δ and γ formulated based on the D_{16} and D_{26} coupling terms:

$$\delta = \frac{D_{26}}{\sqrt[4]{D_{22}^3 \cdot D_{11}}}$$

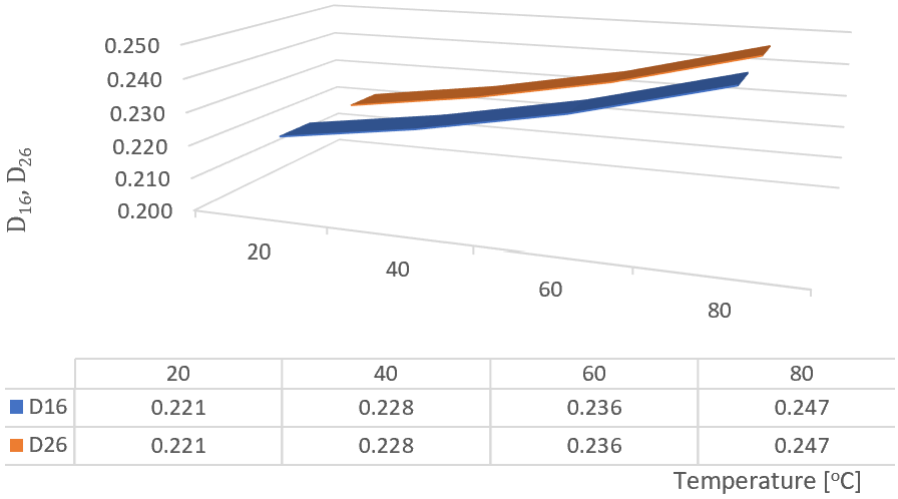
$$\gamma = \frac{D_{16}}{\sqrt[4]{D_{11}^3 \cdot D_{22}}} \tag{3.1}$$

The calculations of those factors for cases presented in this paper has been shown in the Figure 3.8. What is more, in the Figure 3.9 presented the effects of temperature on the coefficients D_{16} and D_{26}. According to Nemeth higher δ value indicates stronger coupling effects, which are closely correlated with deviations in classical buckling patterns and the emergence of complex mode shapes. It should also be remembered that as the temperature increases, the material properties also change and the values of the individual matrix components are strongly dependent on the material properties [32,33]. More observations connected with this phenomenon presented in [51].



a) b)

FIGURE 3.8. Effects of temperature on nondimensional flexural anisotropy parameters: a) δ, b) γ



	20	40	60	80
D16	0.221	0.228	0.236	0.247
D26	0.221	0.228	0.236	0.247

FIGURE 3.9. Effects of temperature on the coefficients D_{16} and D_{26}

The experimental results indicate that temperature modifies not only the magnitude of the critical buckling load but fundamentally reshapes the instability mechanism itself. The transitions between buckling modes arise from the temperature-dependent evolution of flexural–torsional coupling in the laminate. As temperature increases, matrix softening alters the balance of transverse and shear stiffness components, which increases the relative contribution of anisotropic deformation mechanisms and results in a monotonic growth of the coupling terms D_{16} and D_{26}.

Figure 3.8 shows that both nondimensional anisotropy parameters δ and γ increase with temperature, confirming the strengthening of anisotropic coupling effects. This trend is fully consistent with the behaviour of the coupling stiffness components D_{16} and D_{26}, which also rise with increasing temperature, as illustrated in Fig. 3.9. The amplification of coupling interactions modifies the energetic balance between competing deformation modes, leading to abrupt jumps in the equilibrium path when the system shifts to a more energetically favourable configuration.

Thus, the observed mode transitions result from thermally induced changes in anisotropic stiffness, rather than from geometric imperfections alone.

Overall, temperature is a key factor influencing the buckling mechanism. At low temperatures, deformations are more complex and stable, whereas at higher temperatures, initial deformations are simpler but more susceptible to sudden changes and asymmetry. These differences are crucial for the design of structural components that must withstand a wide range of temperatures and loads.

The combined interpretation of the temperature-dependent ABD matrices and the DIC-derived deformation fields demonstrates that temperature fundamentally reshapes the instability

landscape of the composite profile. At low temperatures, the smaller values of D_{16} and D_{26} result in weaker bending–twisting coupling and a more stable deformation pattern dominated by a single preferred buckling mode. At elevated temperatures, softening of the polymer matrix increases laminate anisotropy and amplifies the coupling coefficients D_{16} and D_{26}. This enhancement promotes stronger interaction between bending and twisting, reduces the energetic separation between competing deformation paths and leads to earlier and more frequent mode-switching events. As a consequence, temperature influences not only the magnitude of the critical buckling load but also the structure, multiplicity and stability of the resulting buckling modes.

4. Conclusions

The analysis of results across temperatures ranging from -20°C to 80°C confirmed the significant influence of temperature on the buckling mode, critical buckling load, and aspects related to the reliability and operational performance of compressed composite profiles. Temperature variations modify deformation mechanisms and reduce the material's strength properties, which is crucial for the design and durability of composite structures.

The obtained results confirm:

- **Buckling Mode Variability:** Displacement graphs suggest that increasing temperature leads to a some changes in the buckling mode of composite profiles. Jumps observed in the displacement curves indicate transitions between different buckling patterns, highlighting a reduction in structural stiffness with rising temperature.
- **Effect of Temperature on Critical Buckling Load:** A comparison of graphs across different temperatures reveals a decrease in the critical buckling load at higher temperatures, aligning with theoretical predictions of material strength reduction in elevated temperatures. As temperature increases, structural stiffness decreases, leading to a change in the deformation mode and a reduction in load-bearing capacity.
- **Deformation Asymmetry:** At higher temperatures, deformation asymmetry becomes more pronounced, suggesting an uneven stress distribution and additional thermal effects influencing local buckling behavior.

Additionally, based on the conducted research and obtained results, the following conclusions can be drawn regarding operational aspects:

- **Structural Design:** The impact of temperature on the mechanical properties of composites must be considered, particularly in applications exposed to a wide range of temperatures, to ensure adequate load-bearing capacity and structural stability.

- **Condition Monitoring:** For structures operating at elevated temperatures, regular monitoring of deformations and material condition is recommended to detect early signs of potential buckling-related failures.
- **Material Selection:** Choosing composite materials with higher resistance to temperature variations can enhance structural reliability and durability, minimizing the risk of premature buckling.

These findings provide valuable insights into the behavior of composite profiles under varying thermal conditions, which is crucial for the design and operation of such structures. From a reliability perspective, the results emphasize the necessity of accounting for temperature effects on the mechanical properties of composite materials to ensure safety and durability in fluctuating environmental conditions.

5. Limitations and methodological considerations

From a practical design perspective, uncertainties in material properties, laminate quality, boundary conditions, and initial imperfections can have a pronounced effect on buckling loads and mode transitions. A full variance-based uncertainty analysis would therefore be highly desirable. However, such an investigation would require a substantially larger set of specimens and an extensive numerical campaign, and is beyond the scope of the present experimentally focused study. The current results should thus be viewed as a reference dataset and mechanistic baseline for future UQ-oriented research.

Recent developments in physics-informed and variational deep-learning frameworks, such as Deep Energy Methods and neural operators, offer a promising route to combine experimental data with probabilistic descriptions of input parameters and to quantify output uncertainty directly at the model level. The experimental database established in this work can intended to provide the foundation for such future studies based on machine learning.

Data Availability Statement: The some part of data that support the findings of this study are available [32,33].

Acknowledgement: This research was funded in part by the National Science Centre Poland under the project UMO-2022/47/B/ST8/00600. For the purpose of Open Access, the author has applied a CC-BY public copyright licence to any Author Accepted Manuscript (AAM) version arising from this submission.

The author gratefully acknowledges the valuable guidance and support of prof. Ch. B. York from the Singapore Institute of Technology during the Bekker Fellowship stay. The knowledge

gained during the fellowship under project No. BPN/BEK/2024/1/00229/U/00001, financed by the Polish National Agency for Academic Exchange, was utilized in this research.

K. Falkowicz: Conceptualization, Writing – original draft, Writing – review & editing, Software, Algorithm, Methodology, Experimental test, Investigation, Formal analysis, Validation, Data curation. **P. Wysmulski:** Writing – review & editing, Methodology, Experimental test, Investigation, Analysis and Validation, Data curation.

References

[1] Puig L, Barton A, Rando N. A review on large deployable structures for astrophysics missions. Acta Astronautica 2010;67:12–26. https://doi.org/10.1016/j.actaastro.2010.02.021.

[2] Czyż Z, Podolak P, Skiba K, Jakubczak P, Karpiński P, Różylo P, et al. Autogyro Main Rotor Blade Strength Tests. 2023 IEEE 10th International Workshop on Metrology for AeroSpace (MetroAeroSpace), Milan, Italy: IEEE; 2023, p. 199–204. https://doi.org/10.1109/MetroAeroSpace57412.2023.10190031.

[3] Gao J-X, An Z-W, Ma Q, Bai X-Z. Residual strength assessment of wind turbine rotor blade composites under combined effects of natural aging and fatigue loads. Eksploatacja i Niezawodność – Maintenance and Reliability 2020;22:601–9. https://doi.org/10.17531/ein.2020.4.3.

[4] Kopecki T, Mazurek P, Lis T, Chodorowska D. Post-buckling deformation states of semi-monocoque cylindrical structures with large cut-outs under operating load conditions. Numerical analysis and experimental tests. EiN 2016;18:16–24. https://doi.org/10.17531/ein.2016.1.3.

[5] Kopecki T, Mazurek P. Numerical representation of post-critical deformations in the processes of determining stress distributions inclosed multi-segment thin-walled aircraft load-bearing structures. Eksploatacja i Niezawodność – Maintenance and Reliability 2014;1:163–9.

[6] Buchacz A, Baier A, Herbuś K, Ociepka P, Grabowski Ł, Sobek M. Compression studies of multi-layered composite materials for the purpose of verifying composite panels model used in the renovation process of the freight wagon's hull. Eksploatacja i Niezawodność – Maintenance and Reliability 2018;20:137–46. https://doi.org/10.17531/ein.2018.1.18.

[7] Chróścielewski J, Miśkiewicz M, Pyrzowski Ł, Rucka M, Sobczyk B, Wilde K. Modal properties identification of a novel sandwich footbridge – Comparison of measured dynamic response and FEA. Composites Part B: Engineering 2018;151:245–55. https://doi.org/10.1016/j.compositesb.2018.06.016.

[8] Chróścielewski J, Ferenc T, Mikulski T, Miśkiewicz M, Pyrzowski Ł. Numerical modeling and experimental validation of full-scale segment to support design of novel GFRP footbridge. Composite Structures 2019;213:299–307. https://doi.org/10.1016/j.compstruct.2019.01.089.

[9] Falkowicz K, Kulisz M. Prediction of Buckling Behaviour of Composite Plate Element Using Artificial Neural Networks. Adv Sci Technol Res J 2024;18:231–43. https://doi.org/10.12913/22998624/177399.

[10] Nima SJ, Ganesan R. Buckling analysis of symmetrically laminated composite plates including the effect of variable pre-stress field using the Ritz method. European Journal of Mechanics - A/Solids 2021;90:104323. https://doi.org/10.1016/j.euromechsol.2021.104323.

[11] Chen Q, Qiao P. Buckling and postbuckling of rotationally-restrained laminated composite plates under shear. Thin-Walled Structures 2021;161:107435. https://doi.org/10.1016/j.tws.2021.107435.

[12] Kumar S, Kant L, Poddar MK, Yadav CBK, Kumar S. A review on buckling of the laminated composite panel under in-plane load. Eng Res Express 2024;6:022101. https://doi.org/10.1088/2631-8695/ad3893.

[13] Liang K, Li Z. Postbuckling analysis and optimization of composite laminated panels using a novel perturbation-based approximation FE method. Thin-Walled Structures 2021;160:107398. https://doi.org/10.1016/j.tws.2020.107398.
[14] Namdar Ö, Darendeliler H. Buckling, postbuckling and progressive failure analyses of composite laminated plates under compressive loading. Composites Part B: Engineering 2017;120:143–51. https://doi.org/10.1016/j.compositesb.2017.03.066.
[15] Falkowicz K. Experimental and Numerical Analysis of Compression Thin-Walled Composite Plates Weakened by Cut-Outs. Archives of Civil Engineering 2017;63:161–72. https://doi.org/10.1515/ace-2017-0047.
[16] Falkowicz K, Debski H. The work of a compressed, composite plate in asymmetrical arrangement of layers, Depok, Indonesia: 2019, p. 020005. https://doi.org/10.1063/1.5092008.
[17] Wysmulski P, Debski H. The effect of eccentricity of load on the behavior of compressed composite columns in critical state. Polymer Composites 2019;40:70–7. https://doi.org/10.1002/pc.24601.
[18] Dębski H. Experimental investigation of post-buckling behavior of composite column with top-hat cross-section. Science and Technology 2013.
[19] Mania RJ, Madeo A, Zucco G, Kubiak T. Imperfection sensitivity of post-buckling of FML channel section column. Thin-Walled Structures 2017;114:32–8. https://doi.org/10.1016/j.tws.2017.01.033.
[20] Ehrhardt DA, Virgin LN. Experiments on the thermal post-buckling of panels, including localized heating. Journal of Sound and Vibration 2019;439:300–9. https://doi.org/10.1016/j.jsv.2018.08.043.
[21] Murphy KD, Ferreira D. Thermal buckling of rectangular plates. International Journal of Solids and Structures 2001;38:3979–94. https://doi.org/10.1016/S0020-7683(00)00240-7.
[22] Correia JR, Gomes MM, Pires JM, Branco FA. Mechanical behaviour of pultruded glass fibre reinforced polymer composites at elevated temperature: Experiments and model assessment. Composite Structures 2013;98:303–13. https://doi.org/10.1016/j.compstruct.2012.10.051.
[23] Mazzuca P, Firmo JP, Correia JR, Castilho E. Influence of elevated temperatures on the mechanical properties of glass fibre reinforced polymer laminates produced by vacuum infusion. Construction and Building Materials 2022;345:128340. https://doi.org/10.1016/j.conbuildmat.2022.128340.
[24] Reis JML, Coelho JLV, Monteiro AH, Da Costa Mattos HS. Tensile behavior of glass/epoxy laminates at varying strain rates and temperatures. Composites Part B: Engineering 2012;43:2041–6. https://doi.org/10.1016/j.compositesb.2012.02.005.
[25] Chowdhury EU, Eedson R, Bisby LA, Green MF, Benichou N. Mechanical Characterization of Fibre Reinforced Polymers Materials at High Temperature. Fire Technol 2011;47:1063–80. https://doi.org/10.1007/s10694-009-0116-6.
[26] Gutiérrez Álvarez J, Bisagni C. A Study on Thermal Buckling and Mode Jumping of Metallic and Composite Plates. Aerospace 2021;8:56. https://doi.org/10.3390/aerospace8020056.
[27] Falkowicz K, Kuciej M, Świech Ł. Temperature Effect on Buckling Properties of Thin-Walled Composite Profile Subjected to Axial Compression. Adv Sci Technol Res J 2024;18:305–13. https://doi.org/10.12913/22998624/186607.
[28] Álvarez JG, Bisagni C. Investigation on buckling and mode jumping of composite plates under thermomechanical loads. International Journal of Non-Linear Mechanics 2022;138:103837. https://doi.org/10.1016/j.ijnonlinmec.2021.103837.
[29] Chen X, Nie G, Wu Z. Application of Rayleigh-Ritz formulation to thermomechanical buckling of variable angle tow composite plates with general in-plane boundary constraint. International Journal of Mechanical Sciences 2020;187:106094. https://doi.org/10.1016/j.ijmecsci.2020.106094.
[30] Ahmad F, Awadh MA, Abas M, Noor S, Hameed A. Optimization of Carbon Fiber Reinforced Plastic Curing Parameters for Aerospace Application. Applied Sciences 2022;12:4307. https://doi.org/10.3390/app12094307.

[31] Dębski H, Bieniaś J. Experimental and Numerical Analysis of Post-Critical States and Damage of Thin-Walled Channel Section Columns Made of Carbon/Epoxy Composite. Adv Sci Technol Res J 2021;15:321–31. https://doi.org/10.12913/22998624/142603.
[32] Falkowicz K. Determined material properties within the framework of the NCN project (OPUS) No. 2022/47/B/ST8/00600 2025. https://doi.org/10.5281/ZENODO.15037571.
[33] Falkowicz K. Material properties of CFRP composite 2025. https://doi.org/10.18150/YKBDJQ.
[34] Bailie JA, Ley RP, Pasricha AA. A summary and review of composite laminate design guidelines. Task 22, NASA Contract NAS1-19347 1997.
[35] York CB. Characterization of Nonsymmetric Forms of Fully Orthotropic Laminates. Journal of Aircraft 2009;46:1114–25. https://doi.org/10.2514/1.32938.
[36] Falkowicz K, Samborski S, Valvo PS. Effects of Elastic Couplings in a Compressed Plate Element with Cut-Out. Materials 2022;15:7752. https://doi.org/10.3390/ma15217752.
[37] Falkowicz K. Validation of Extension-Bending and Extension-Twisting Coupled Laminates in Elastic Element. Adv Sci Technol Res J 2023;17:309–19. https://doi.org/10.12913/22998624/167451.
[38] Jones RM. Mechanics of Composite Materials. 2nd ed. CRC Press; 2018. https://doi.org/10.1201/9781498711067.
[39] York C. Unified approach to the characterization of coupled composite laminates: Hygro-thermally curvature-stable configurations. International Journal of Structural Integrity 2011;2:406–36. https://doi.org/10.1108/17579861111183920.
[40] York CB. On Bending-Twisting coupled laminates. Composite Structures 2017;160:887–900. https://doi.org/10.1016/j.compstruct.2016.10.063.
[41] York CB, Weaver PM. Balanced and symmetric laminates - New perspectives on an old design rule 2010.
[42] Golewski P, Sadowski T, Kneć M, Budka M. The effect of thermal aging degradation of CFRP composite on its mechanical properties using destructive and non-destructive methods and the DIC system. Polymer Testing 2023;118:107902. https://doi.org/10.1016/j.polymertesting.2022.107902.
[43] Wysmulski P, Debski H, Falkowicz K. Sensitivity of Compressed Composite Channel Columns to Eccentric Loading. Materials 2022;15:6938. https://doi.org/10.3390/ma15196938.
[44] Wysmulski P, Debski H, Falkowicz K. Stability analysis of laminate profiles under eccentric load. Composite Structures 2020;238:111944. https://doi.org/10.1016/j.compstruct.2020.111944.
[45] Wysmulski P. Load Eccentricity of Compressed Composite Z-Columns in Non-Linear State. Materials 2022;15:7631. https://doi.org/10.3390/ma15217631.
[46] Wysmulski P. Failure Mechanism of Tensile CFRP Composite Plates with Variable Hole Diameter. Materials 2023;16:4714. https://doi.org/10.3390/ma16134714.
[47] Pickerd V. Optimisation and Validation of the ARAMIS Digital Image Correlation System for use in Large-scale High Strain-rate Events 2013.
[48] Wysmulski P. Analysis of the Effect of an Open Hole on the Buckling of a Compressed Composite Plate. Materials 2024;17:1081. https://doi.org/10.3390/ma17051081.
[49] Hu L, Liang X, Feng P, Li H-T. Temperature effect on buckling behavior of prestressed CFRP-reinforced steel columns. Thin-Walled Structures 2023;188:110879. https://doi.org/10.1016/j.tws.2023.110879.
[50] Nemeth MP. Importance of anisotropy on buckling of compression-loaded symmetriccomposite plates. AIAA Journal 1986;24:1831–5. https://doi.org/10.2514/3.9531.
[51] Falkowicz K. INFLUENCE OF EXTENSION-SHEARING BENDING-TWISTING AND BENDING-TWSTING COUPLING ON THE BUCKLING BEHAVIOUR OF COMPOSITE PROFILES. Acta Mechanica et Automatica 2025.